International Journal of Nanomedicine

Dovepress

open access to scientific and medical research

Open Access Full Text Article

ORIGINAL RESEARCH

Construction and Evaluation of BAL-PTX Co-Loaded Lipid Nanosystem for Promoting the Anti-Lung Cancer Efficacy of Paclitaxel and Reducing the Toxicity of Chemotherapeutic Drugs

Tao Chen[1–3,*], Yumeng Wei[1–3,*], Suyu Yin[1–3,*], Wen Li[1–3], Yuxiang Wang[1–3], Chao Pi[1–3], Mingtang Zeng[3,4], Xiaodong Wang[5], Ligang Chen[6], Furong Liu[7], Shaozhi Fu[8], Ling Zhao[2,3]

[1]Key Laboratory of Medical Electrophysiology, Ministry of Education, School of Pharmacy, Southwest Medical University, Luzhou, 646000, People's Republic of China; [2]Luzhou Key Laboratory of Traditional Chinese Medicine for Chronic Diseases Jointly Built by Sichuan and Chongqing, The Affiliated Traditional Chinese Medicine Hospital, Southwest Medical University; Luzhou, Sichuan, 646000, People's Republic of China; [3]Central Nervous System Drug Key Laboratory of Sichuan Province, School of Pharmacy, Southwest Medical University, Luzhou, Sichuan, 646000, People's Republic of China; [4]Department of Pharmacy, West China Hospital, Sichuan University, Chengdu, 610041, People's Republic of China; [5]Department of Hepatobiliary Diseases, The Affiliated Traditional Chinese Medicine Hospital, Southwest Medical University, Luzhou, Sichuan, 646000, People's Republic of China; [6]Department of neurosurgery, The Affiliated Hospital, Southwest Medical University, Luzhou, Sichuan, 646000, People's Republic of China; [7]Department of Oncology, The Affiliated Traditional Chinese Medicine Hospital, Southwest Medical University, Luzhou, Sichuan, 646000, People's Republic of China; [8]Department of Oncology, The Affiliated Hospital, Southwest Medical University, Luzhou, Sichuan, 646000, People's Republic of China

*These authors contributed equally to this work

Correspondence: Shaozhi Fu, Department of Oncology, The Affiliated Hospital, Southwest Medical University, Luzhou, 646000, People's Republic of China, Tel +86 830-3165698, Fax +86 830-3165690, Email shaozhifu513@163.com; Ling Zhao, Luzhou Key Laboratory of Traditional Chinese Medicine for Chronic Diseases Jointly Built by Sichuan and Chongqing, The Affiliated Traditional Chinese Medicine Hospital, Southwest Medical University, No. 182, Chunhui Road, Longmatan District, Luzhou, Sichuan, 646000, China, Tel +86 830 2681630, Email zhaoling@swmu.edu.cn

Purpose: The present study aimed to develop a lipid nanoplatform, denoted as "BAL-PTX-LN", co-loaded with chiral baicalin derivatives (BAL) and paclitaxel (PTX) to promote the anti-lung cancer efficacy of paclitaxel and reduce the toxicity of chemotherapeutic drugs.

Methods: BAL-PTX-LN was optimized through central composite design based on a single-factor experiments. BAL-PTX-LN was evaluated by TEM, particle size, encapsulation efficiency, hemolysis rate, release kinetics and stability. And was evaluated by pharmacokinetics and the antitumor efficacy studied both in vitro and in vivo. The in vivo safety profile of the formulation was assessed using hematoxylin and eosin (HE) staining.

Results: BAL-PTX-LN exhibited spherical morphology with a particle size of 134.36 ± 3.18 nm, PDI of 0.24 ± 0.02, and with an encapsulation efficiency exceeding 90%, BAL-PTX-LN remained stable after 180 days storage. In vitro release studies revealed a zero-order kinetic model of PTX from the liposomal formulation. No hemolysis was observed in the preparation group. Pharmacokinetic analysis of PTX in the BAL-PTX-LN group revealed an approximately three-fold higher bioavailability and twice longer $t_{1/2}$ compared to the bulk drug group. Furthermore, the IC_{50} of BAL-PTX-LN decreased by 2.35 times (13.48 μg/mL vs 31.722 μg/mL) and the apoptosis rate increased by 1.82 times (29.38% vs 16.13%) at 24 h compared to the PTX group. In tumor-bearing nude mice, the BAL-PTX-LN formulation exhibited a two-fold higher tumor inhibition rate compared to the PTX group (62.83% vs 29.95%), accompanied by a ten-fold decrease in Ki67 expression (4.26% vs 45.88%). Interestingly, HE staining revealed no pathological changes in tissues from the BAL-PTX-LN group, whereas tissues from the PTX group exhibited pathological changes and tumor cell infiltration.

Conclusion: BAL-PTX-LN improves the therapeutic effect of poorly soluble chemotherapeutic drugs on lung cancer, which is anticipated to emerge as a viable therapeutic agent for lung cancer in clinical applications.

Keywords: baicalin derivative, paclitaxel, chemotherapy, lung cancer, lipid nano platform, combination therapy

Received: 15 June 2024
Accepted: 19 July 2024
Published: 30 July 2024

Graphical Abstract

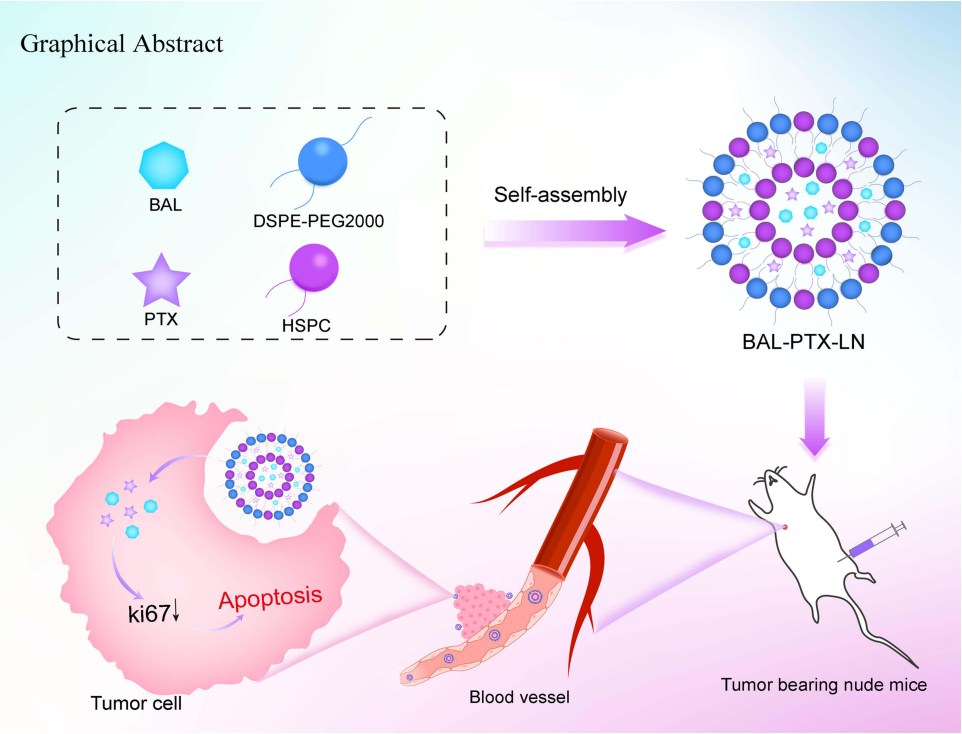

Introduction

The safety of human life is threatened by the serious illness of cancer, with up to 20 million new cases of cancer and nearly 10 million cancer-related deaths reported worldwide.[1,2] Among various types of cancer, lung cancer stands out as particularly lethal, responsible for over 1.8 million deaths annually and constituting 18% of all cancer-related deaths.[3] While treatments such as radiotherapy and surgery offer alternatives, chemotherapy remains the most common approach.[4,5]

Paclitaxel (PTX) is an exemplary chemotherapeutic agent for advanced human cancers and is frequently employed in lung cancer treatment.[6] Commercially available formulations of PTX include injections and albumin nanoparticles. However, the injection formulation, employing Cremophor EL (polyoxyethylene castor oil) and anhydrous ethanol as solubilizing agents, often elicit allergic reactions.[7] Clinical trials with PTX albumin nanoparticles have revealed substantial bone marrow toxicity, gastrointestinal reactions, severe liver injury, and other adverse effects leading to treatment cessation or failure.[8] Combining PTX with various drugs can elicit synergistic effects and mitigate associated adverse effects. For instance, the combination therapy of S-1 (an orally administered fluorouracil derivative) and PTX has shown promising efficacy in previously treated patients with advanced non-small cell lung cancer.[9] Additionally, combining PTX with a CCR7 monoclonal antibody has been shown to delay tumor growth in B16F10 melanoma and reduce lymphatic metastasis.[10] Nintedanib in combination with PTX has demonstrated enhanced overall antitumor activity in both primary and metastatic therapy settings.[11] Natural pharmaceutical monomers such as baicalin, curcumin, and honokiol, when combined with PTX, have been reported to modulate various signaling pathways in cancer cells, mitigate dose-dependent adverse events associated with PTX, improve the quality of life of patients with lung cancer, and enhance therapeutic efficacy.[12–14] Previous studies by our research group have identified a novel compound, BAL, which has potent anti-tumour effects.[15] BAL acts as an inhibitor of the protein kinase B (PKB or Akt) pathway, inducing apoptosis in lung cancer cells while demonstrating significant antitumor activity and safety for normal cells and tissues. PTX, on the other hand, interferes with the normal function of tubulin during cancer cell division, inducing cell cycle

arrest and inhibiting cancer cell proliferation.[16–18] Therefore, combining these two drugs can significantly enhance synergistic anti-lung cancer effects.

The translation of the demonstrated synergistic impact observed in vitro into advantageous outcomes in vivo for lung cancer treatment using a combination of BAL and PTX remains a pivotal challenge to address. A common method of administration is "cocktail" therapy, where two or more medications are physically mixed and administered together.[19] While practical, this approach is fraught with limitations. Variations in medication pharmacokinetics, tissue distribution, and cell membrane permeability lead to inconsistent drug delivery at tumor sites, making it difficult to establish the optimal drug synergy ratio in vitro, often resulting in the failure of combined therapy strategies.[20,21] The inherent challenges of low solubility and poor bioavailability of PTX and BAL persist as fundamental obstacles in the development of clinical therapeutic preparations, despite their significant medicinal value when combined.[15,22,23] To overcome these challenges and improve the characteristics of PTX and various drug combinations, the selection of a suitable co-loading delivery system is imperative. Progress in this area includes the development of solvent-free preparations, scalability assessment, and long-term stability evaluation. The field of cancer treatment has benefited significantly from advancements in nanotechnology and nanomedicine, which have led to increased drug accumulation in tumor tissues and targeted uptake by tumor cells through nano-drug delivery systems. Lipid-based nanoparticles represent a promising avenue for anticancer drug delivery, serving as sophisticated and comprehensive nano-scale delivery systems for diverse bioactive substances.[24,25] These lipid nanocarriers use various functional groups on their surfaces to facilitate the attachment of molecules such as antibodies, polysaccharides, and medications, thereby enhancing drug delivery to cancer cells. Their advantages include rapid absorption, minimal adverse effects, ease of production, and excellent in vivo stability.[26,27] In terms of lipid nanomaterials, Hydrogenated soybean phospholipids (HSPC), as a drug-carrying membrane material, helps to improve drug stability. 1.2-dis-tearoyl-sn-glycero -3-phosphoethanolamine-N-[methoxy (poly-ethylene glycol)-2000] (DSPE-PEG2000) can encapsulate the drug through hydrophobic interactions while the PEG macromolecule extends on the surface of the lipid membrane to achieve a high degree of hydration and enhance drug uptake, which is easier to synthesize than liposomal nanomaterials, such as cholesterol, and has pharmacokinetic characteristics more suitable for use in vivo as a drug carrier.

In this study, PTX was combined with BAL for the first time, and the synergistic effect of BAL-PTX was investigated and screened at the cellular level. To further enhance its efficacy, a lipid nano-drug delivery system was utilized to co-load the two drugs into the same system. The effects against lung cancer of the co-loaded BAL and PTX lipid nano-system were investigated both in *vitro* and in vivo, and their pharmacokinetic behavior was evaluated. It is anticipated that this drug co-delivery system will mitigate toxicity to major organs, improve the delivery of poorly soluble chemotherapeutic medications, and enhance the therapeutic efficacy against lung cancer.

Materials and Methods

Materials

Baicalin (BA, purity ≥ 98%) and paclitaxel (PTX, purity ≥ 98%) were purchased from Chengdu Best Reagent Co., Ltd (China). HSPC and DSPE-PEG2000 were purchased from Lipoid GmbH (Germany). Methylthiazolyldiphenyl-tetrazolium bromide (MTT) were purchased from Beijing Solarbio Science&Technology Co., Ltd (China). All other chemicals were of chromatographic grade.

Cell Lines and Cultures

Human lung cancer cells (A549 and H460) were obtained from the Tumor Cell Bank of the Chinese Academy of Medical Sciences, and the normal liver cells (L02) were obtained from the Basic Medicine Laboratory of the Affiliated Hospital of Southwest Medical University (Sichuan, China). All cell lines were maintained in RPMI 1640 or DMEM (Gibco; Thermo Fisher Scientific, USA) with 10% fetal bovine serum (Hyclone, Utah, USA) and 100 U/mL penicillin-streptomycin in a humidified environment with 5% CO2 at 37°C.

Combination Index of BAL-PTX at Various Ratios

The cell proliferation kit (MTT colorimetric method) was used to assess the toxicity of several drugs to H460, A549, and L02 cells. When the cells approach the logarithmic growth stage, they are counted, and quantitative fresh culture medium is added to prepare a cell suspension with the desired concentration. Cells were seeded at a density of $3–5\times10^3$ cells/well in a 96-well plate. The cells were cultured in an incubator at 5% CO2 and 37°C for 24 hours before different quantities of medicines were added to a 96-well plate. After drug intervention for 24, 48, 72, or 96 h, 20 μL of MTT solution (5 mg/mL) was added to each well, and the culture was terminated after incubation for 3–4 hours, and 150 μL of DMSO was added after the medium was sucked out. In order to fully dissolve the crystal, shake it for 10 min. Subsequently, the optical density (OD) of each well was measured with a microplate at a wavelength of 490 nm. The growth inhibition rate of drugs on cells was calculated according to the formula:

$$\text{Inhibition rate}(\%)=[1-(\text{OD experiment}-\text{OD blank})/(\text{OD control}-\text{OD blank})]\times 100\%$$

In order to screen the combined effects of different concentration ratios of BAL:PTX, A549 and H460 cells were incubated in 96-well plates, and the drugs with concentration ratios of BAL:PTX (μg/μg) of 80:1, 20:1, 5:1, 2:1, and 1:1 were used for intervention, respectively. The MTT assay was used to quantify the inhibition rate of cell growth. Combination index (CI) based on median effect analysis.[28] CI > 1, CI = 1, and CI < 1 indicate antagonism, addition, and synergy, respectively.[29,30]

Preparation, Optimization, and Characterization of BAL-PTX-LN

Preparation of BAL-PTX-LN

Accurately weigh the prescribed amount of PTX, BAL, HSPC (35 mg), and DSPE-PEG2000 (10 mg) in a round-bottomed flask and dissolve it in 3 mL of chloroform. The solvent was removed by vacuum distillation with a rotary evaporator at 37°C for 6 minutes at a speed of 160 rpm, and a lipid film formed on the inner wall of the flask. Nitrogen is injected to ensure that there is no leftover solvent, and it is then placed in a 37°C oven for roughly 2 hours. After adding distilled water for hydration, the nanoparticles were evenly dispersed by an ultrasonic cell crusher (160 W, 6 min) to obtain clear BAL-PTX-LN. For long-term storage, 1% sucrose (w/v) was added, and yellow-green loose powder was obtained after freeze-drying for about 24 hours.

Optimization of BAL-PTX-LN

A single-factor experiment was used to evaluate the preparation technique (ultrasonic intensity and time) and prescription (HSPC, DSPE-PEG2000, and the dosage of the drugs). The BAL-PTX-LN prescription was then designed and optimized using the central composite design-response surface method. Each step of the screening process uses the particle size, PDI, and encapsulation efficiency of lipid nanoparticles as evaluation indexes.

Characterization of BAL-PTX-LN

Particle size, PDI (representing uniformity of particle size distribution) and Zeta potential were measured at 25°C using a Malvern particle size analyzer. The morphology of the sample was examined by using a transmission electron microscopy (TEM).

To measure the encapsulation efficiency, put 100 μL of BAL-PTX-LN lipid nanoparticle solution into a centrifuge tube, add 5 mL of methanol to decompose the nanoparticles, dilute them properly, and then ultrasonic for 4 minutes. The content was tested by HPLC following centrifugation (8000 rpm, 10 min), and the concentration was C2. Moreover, after properly measuring 100 μL of BAL-PTX-LN lipid nano-particle solution, remove the leftover nano-solution, centrifuge (8000 rpm, 10 min), and measure 100 μL of supernatant. HPLC is used to determine the concentration of C1. The following is the entrapment efficiency (EE) formula:

$$\text{EE}(\%)=\text{C1}/\text{C2}\times 100\%$$

In vitro Antitumor Investigation of BAL-PTX-LN

The MTT colorimetric method was used to assess the toxicity of BAL-PTX and BAL-PTX-LN to H460, A549, and L02 cells. As for the apoptosis experiment, A549 cells were inoculated into a 6-well plate at a density of 3×10^5 cells per well and adhered to the wall overnight. When the cells grew to 70–80%, they were given three kinds of drug solutions with high (20 μg/mL), medium (10 μg/mL), and low (5 μg/mL) concentrations, respectively, and a blank control group was set up. After 24 h of drug action, all cells were digested and collected, washed twice with PBS, and counted. Add 500 μL of binding buffer to the collected 6×10^5 cells, blow the cells evenly, and then transfer them to a 5 mL detection tube. At room temperature and in the dark, 5 μL of Annexin V/FITC and 5 μL of PI were added successively, and then they were fully mixed and dyed.

In vitro Release Behavior of BAL-PTX-LN

The BAL-PTX-LN release curve was studied using PBS phosphate buffer solution in a total volume of 120 mL as the release medium. Fill dialysis bags (8000–14000 Da) with 2 mL of BAL-PTX-LN and 2 mL of BAL-PTX at the same medication concentration (1 mg/mL). The release test was performed in the dissolution apparatus at 37°C and 100 rpm. At 0.08 h, 0.25 h, 0.5 h, 1 h, 2 h, 4 h, 8 h, 12 h, 24 h, and 48 h, 2 mL of dialysate was removed and replaced with the same amount of release medium to keep the total volume constant. The peak area of the drug in the supernatant was evaluated by HPLC after centrifuging the dialysate, and the cumulative release rate at different intervals was computed using the standard curve, and the in vitro release curve was created.

The Stability Evaluation of BAL-PTX-LN

Investigation of Solution Stability

Three batches of BAL-PTX-LN solution were prepared according to the optimized formula and process, and their stability was investigated by taking the encapsulation efficiency, particle size, and PDI as indexes under the conditions of 25 ± 2°C and 4 ± 2°C.

Investigation on Long-Term Stability of Freeze-Dried Powder

Three batches of BAL-PTX-LN freeze-dried powder were prepared according to the optimized formula and technology and placed at 25 ± 2°C and 40 ± 5% relative humidity. Samples were taken at the end of the 1st, 2nd, 3rd, 6th, 9th, and 12th month, respectively. After the sample was dissolved in deionized water, the particle size, PDI and encapsulation efficiency were detected, and the long-term stability of the sample was investigated by comparing with the beginning.

In vitro Hemolytic Analysis

Fibrinogen was destroyed by taking 2 mL of blood from Sprague Dawley (SD) rats and stirring clockwise through a glass rod for 5 min. Add an appropriate amount of 0.9% sodium chloride solution, centrifuge with stirring (1500 rpm, 10 min) and pour out the supernatant. To obtain erythrocytes, continue to add 0.9% sodium chloride solution and repeat the shaking and centrifugation process described above until the supernatant is colorless. Add 2% erythrocyte suspension to 0.9% sodium chloride solution. BAL-PTX-LN, negative control (2% physiological saline) and positive blank control (ultrapure water) were put into the incubator at 37°C for hemolysis test, and the groups are shown in the table below. Hemolysis was assessed in all groups after centrifugation (1500 rpm, 10 min). After 5 h, the supernatant of each sample was added to a 96-well plate. At the wavelength of 540 nm, the absorbance (A) was measured by an enzyme-labeled instrument, and then the hemolysis rate (%) was calculated according to the following formula:

$$\text{Hemolysis}(\%)=(\text{A sample}-\text{A negative})/(\text{A positive}-\text{A negative})\times100\%$$

Pharmacokinetic Studies

Ten SD rats were randomly assigned to one of two groups: (1) the BAL-PTX raw material medication group and (2) the BAL-PTX-LN preparation group. The concentrations of PTX and BAL in both groups were 10 mg/kg and 50 mg/kg, respectively. After administration, cardiac blood samples were obtained from each rat at 5, 10, 15, 30, 60, 120, 240, 480,

720, 1440, and 2880 min. The original blood (0.3 mL) was centrifuged for 3 minutes at 5000 rpm/min in a centrifuge tube containing heparin sodium, and the plasma sample was treated before being detected by HPLC.

In vivo Tumor Efficacy and Safety Study of the Drug Combination

The experiment terminated after 21 days of treatment, and the surviving nude mice were killed, the tumor mass was taken out and weighed, and the tumor inhibition rate was calculated. Each group's subcutaneous tumor tissues and related organ tissues were washed twice with 0.9% physiological saline before being fixed with an adequate amount of 4% paraformaldehyde solution. The fixed tissues were dehydrated before being embedded in paraffin and sliced. Following that, the pathological sections of the subcutaneous transplanted tumor, heart, lung, and kidney were then stained with hematoxylin and eosin (HE) and evaluated.

Immunohistochemistry

After the tumor tissue was fixed with 4% paraformaldehyde for 24 h, it was dehydrated with absolute alcohol and embedded in paraffin to prepare tumor sections. The antigen was recovered for 5 min in the high-temperature environment of 0.01 M citric acid buffer (pH = 6.0). The first antibody (1:200) was added dropwise at 4 °C, then cultured overnight, and then the second antibody was added dropwise at 37 °C for 30 min. Finally, the slices were colored by 3, 3'-diaminobenzidine and stained with hematoxylin, and then the images were collected by a micro-camera system. All experimental procedures were carried out by blind method.

Statistical Analysis

All data were obtained using the GraphPad Prism 8.0 statistical package. Data were expressed as mean ± standard deviation in triplicate. Differences among multiple groups were determined using the Student's *t*-test or one-way ANOVA with a post hoc test and considered statistically significant at $P < 0.05$.

Results

Synergistic Effects of BAL-PTX

The IC_{50} values of free PTX and BAL solution on lung cancer cell A549 were 45.863 μg/mL and 40.571 μg/mL, respectively, at 24 h (Figure 1A and Table 1). When BAL and PTX were combined, the inhibitory rate of BAL-PTX on lung cancer cell A549 was significantly higher than that of PTX or BAL alone across various proportions at any given dose and time point. Notably, at a mass ratio of 5:1, the BAL-PTX group exhibited the lowest IC_{50} value among all, measuring 24.398 μg/mL at 24 h and 16.022 μg/mL at 48 h. The analysis results of the CI are depicted in Figure 1B and Table 2. For the effective dose 50 (ED_{50}), the CI of BAL-PTX was less than 1 for all mass ratios at both 24 and 48 h. In particular, at a mass ratio of 5:1, BAL-PTX demonstrated the lowest CI value of 0.323 at 24 h. However, for ED_{75} and ED_{90}, the CI of BAL-PTX at mass ratios of 80:1, 2:1, and 1:1 at 24 h exceeded 1. Nevertheless, after 48 h, the situation notably improved, with the CI of BAL-PTX being less than 1 for nearly all mass ratios. The dose-effect curve clearly indicates that BAL-PTX, with a mass ratio of 5:1, exhibits superior cell inhibition at the same dosage.

Similarly, for H460 lung cancer cells, the inhibition rate of BAL plus PTX was significantly higher than that of PTX or BAL alone across various ratios and concentrations at 24 h. Moreover, we observed that the inhibition rate of BAL-PTX on H460 cells was notably higher at a mass ratio of 5:1 compared to other ratios. After 48 h, the IC_{50} values of the BAL-PTX combination were only 14.86 μg/mL for the 5:1 group and 18.304 μg/mL for the 2:1 group, both lower than the IC_{50} values of the BAL single drug group, which was 21.854 μg/mL (Figure 1C and Table 3). The analysis results of the drug combination index are presented in Figure 1D and Table 4. At 48 h, the CI of BAL-PTX for all mass ratios for ED_{50}, ED_{75}, and ED_{90} was < 1. Notably, while the CI of BAL-PTX exceeded 1 in many proportions at 24 h, the CI values of BAL-PTX with a mass ratio of 5:1 for ED_{50} (0.193), ED_{75} (0.274), and ED_{90} (0.393) were all less than 1, indicating good synergy. In particular, at 48 h, several CI values of BAL-PTX with a mass ratio of 5:1 were among the smallest compared to other mass ratios at the same lethal dose.

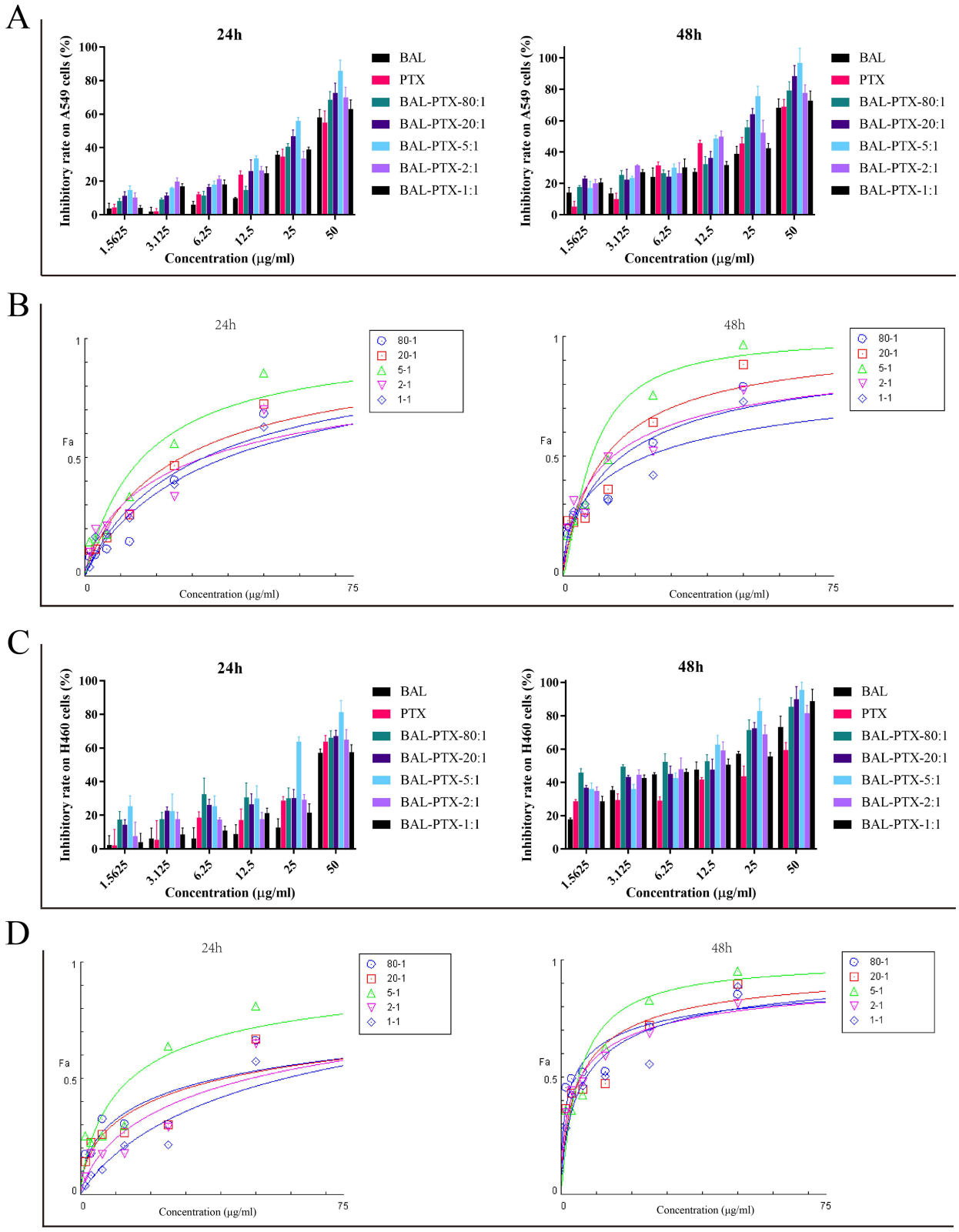

Figure 1 MTT experimental results of API combination. The inhibition rate (%) of PTX, BAL and different ratios of BAL-PTX on A549 cells at 24 h and 48 h (**A**). Dose-response curves for BAL-PTX with various BAL: PTX mass ratios in the A549 cell growth inhibition trials (**B**). The inhibition rate (%) of PTX, BAL and different ratios of BAL-PTX on H460 cells at 24 h and 48 h (**C**). Dose-response curves for BAL-PTX with various BAL: PTX mass ratios in the H460 cell growth inhibition trials (**D**). ($\bar{x} \pm s$, n = 4).

Table 1 IC_{50} Values of BAL, PTX and BAL-PTX Against A549 Tumor Cells

IC_{50} (μg/mL)	Time	
	24 h	48 h
BAL	40.571	38.512
PTX	45.863	31.722
BAL-PTX (80:1)	35.754	28.987
BAL-PTX (20:1)	30.979	23.571
BAL-PTX (5:1)	24.398	16.022
BAL-PTX (2:1)	40.353	26.399
BAL-PTX (1:1)	36.083	39.027

Table 2 The Combination Index Values of BAL: PTX in A549 Cells

Time	Mass Ratio	Combination Index Values		
		ED_{50}	ED_{75}	ED_{90}
24 h	80:1	0.767	1.011	1.332
	20:1	0.527	0.708	0.953
	5:1	0.323	0.377	0.439
	2:1	0.690	1.216	2.143
	1:1	0.710	0.891	1.120
48 h	80:1	0.515	0.464	0.421
	20:1	0.375	0.275	0.206
	5:1	0.270	0.148	0.086
	2:1	0.504	0.661	0.921
	1:1	0.907	1.837	3.908

Table 3 IC_{50} Values of BAL, PTX and BAL-PTX Against H460 Tumor Cells

IC_{50} (μg/mL)	Time	
	24 h	48 h
BAL	47.961	21.854
PTX	49.27	39.402
BAL-PTX (80:1)	47.839	29.55
BAL-PTX (20:1)	44.757	24.191
BAL-PTX (5:1)	27.029	14.86
BAL-PTX (2:1)	43.412	18.304
BAL-PTX (1:1)	49.622	30.279

Preparation, Optimization, and Characterization of BAL-PTX-LN

Single Factor Experiment

Initially, we explored the preparation factors influencing the quality of BAL-PTX-LN via single-factor experiments. Particle size (124.85 ± 7.12 nm), polydispersity index (PDI) (0.258 ± 0.012), and encapsulation efficiency (EE) (BAL: 92.35 ± 3.30%, PTX: 94.35 ± 4.23%) of the preparation reached their optimal values under each ultrasonic intensity

Table 4 The Combination Index Values of BAL: PTX in H460 Cells

Time	Mass ratio	Combination index values		
		ED_{50}	ED_{75}	ED_{90}
24 h	80:1	0.432	1.027	2.445
	20:1	0.475	1.052	2.343
	5:1	0.193	0.274	0.393
	2:1	0.774	1.240	2.012
	1:1	1.077	1.363	1.742
48 h	80:1	0.309	0.469	0.714
	20:1	0.449	0.366	0.301
	5:1	0.369	0.180	0.292
	2:1	0.356	0.380	0.441
	1:1	0.401	0.589	0.693

when the intensity was set at 160 W (Figure 2B). Optimal ultrasonic time for producing BAL-PTX-LN was determined to be 6 min because the particle size of the preparation and PDI were acceptable at this duration (Figure 2A). Subsequently, we investigated the prescription factors of BAL-PTX-LN (BAL-PTX, HSPC, and DSPE-PEG2000) individually, and the results are depicted in Figures 2C–E. Following a comprehensive assessment, tentative prescriptions were established as follows: BAL-PTX (5 mg), HSPC (35 mg), and DSPE-PEG2000 (10 mg), utilizing EE, drug loading (DL), and PDI as indices. Under these conditions, BAL-PTX-LN was produced with a particle size of 131.47 ± 7.02 nm and a PDI of 0.243 ± 0.011, with EE (BAL: 93.90 ± 5.02%, PTX: 94.26 ± 4.55%).

Furthermore, we evaluated the impact of sucrose, lactose, and mannitol as freeze-drying protectants on the quality of the freeze-dried powder of BAL-PTX-LN. Particle size, PDI, and EE of BAL-PTX-LN before and after freeze-drying did not significantly differ when sucrose was employed as the cryoprotectant ($P > 0.05$). The encapsulation effectiveness is greater than 90%, the particle size is around 130 nm, and the PDI is approximately 0.25. Particle size and PDI both prior to and following freeze-drying are more appropriate, and encapsulation efficiency is increased. As a result, sucrose was chosen as the protective agent for freeze-drying.

Optimization of BAL-PTX-LN

Three factors were selected as research objects: BAL-PTX content (X1), HSPC content (X2), and DSPE-PEG2000 (X3). Central composite design (CCD) was employed to optimize the preparation prescription. Utilizing particle size, PDI, and EE as evaluation indexes, dependent variables (Y1, Y2, and Y3) were fitted using polynomial algorithms and multiple linear regression, respectively, through the statistical program Expert Design 10.0. The accuracy of the regression equation was evaluated using statistical indicators, including F-test, lack-of-fit, and R-squared. The equation obtained by fitting is as given below:

$$Y1 = +145.06 + 21.51 * X1 + 8.69 * X237.80 * X3 + 53.75 * X1 * X2 + 14.33 * X1 * X3 - 27.63 * X2 * X3 + 49.97 * X1^2 + 9.32 * X2^2 + 45.75 * X3^2$$

$$Y2 = +0.26 + 0.007 * X1 + 0.007 * X2 - 0.026 * X3 + 0.049 * X1 * X2 - 0.004 * X1 * X3 - 0.010 * X2 * X3 + .063 * X1^2 + 0.009 * X2^2 + 0.044 * X3^2$$

$$Y3 = +95.10 - 4.74 * X1 + 1.85 * X2 + 4.46 * X3 + 1.20 * X1 * X2 + 2.97 * X1 * X3 + 7.90 * X2 * X3 - 5.36 * X1^2 - 11.14 * X2^2 - 6.76 * X3^2$$

The Y1, Y2, and Y3 equation's fitting degree (R^2) indicates that the particle size, PDI, and encapsulation efficiency have well-fitting outcomes. A robust mathematical equation model exists for the three indices of BAL-PTX-LN

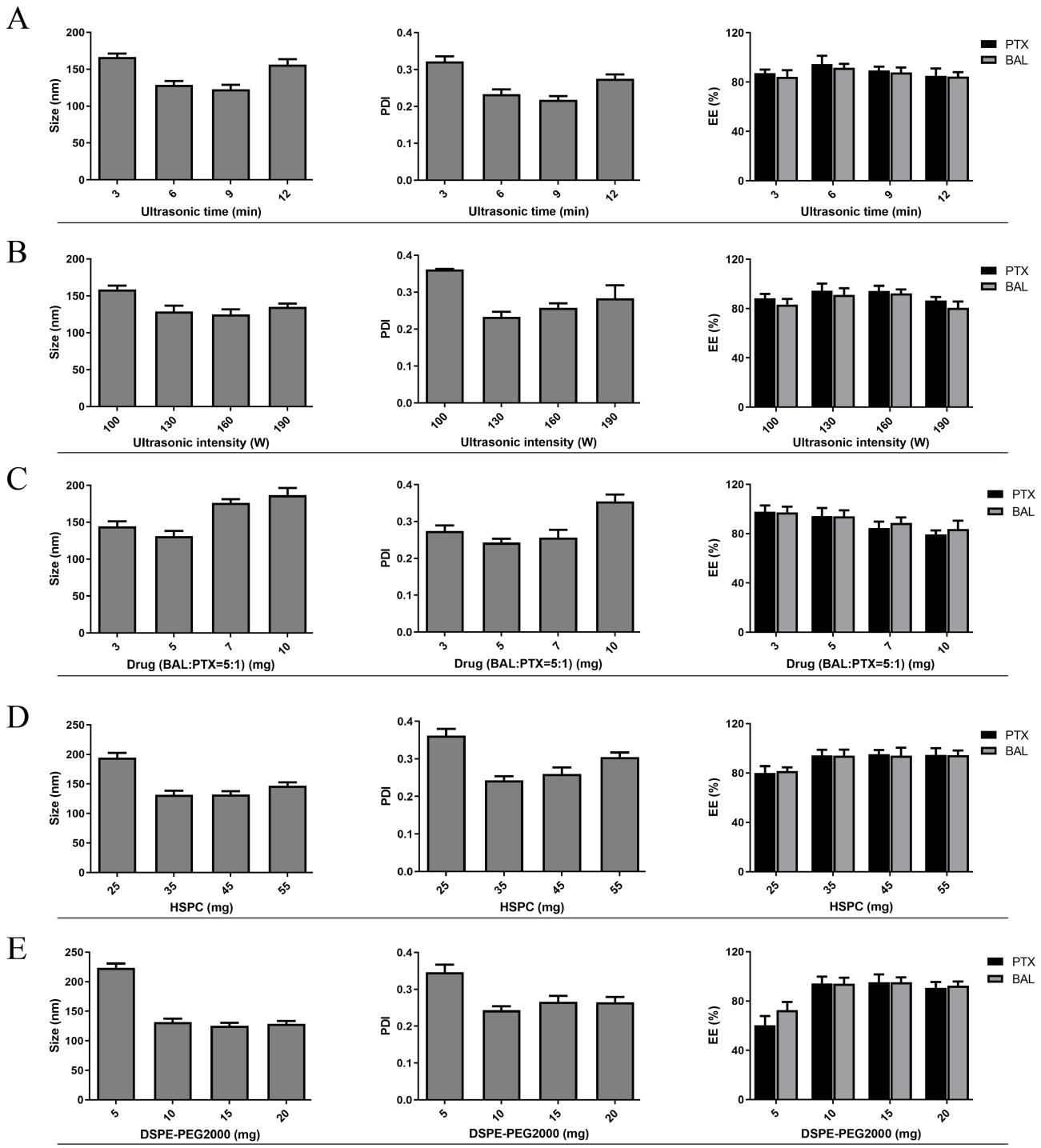

Figure 2 The results of single factor investigation. The effects of different ultrasonic time on the particle size, PDI and encapsulation efficiency of lipid nanoparticles (**A**). The effects of different ultrasonic intensity on the particle size, PDI and encapsulation efficiency of lipid nanoparticles (**B**). The effects of different main drug contents on the particle size, PDI and encapsulation efficiency of lipid nanoparticles (**C**). The effects of different HSPC contents on the particle size, PDI and encapsulation efficiency of lipid nanoparticles (**D**). The effects of different DSPE-PEG2000 contents on the particle size, PDI and encapsulation efficiency of lipid nanoparticles (**E**).

preparation as well as the prescription parameters requiring optimization. Ultimately, we used three components and three levels to meet the experimental design. Figure 3 displays the response surface contour map results. The information indicates that the main drugs, HSPC and DSPE-PEG2000, have a significant impact on the encapsulation efficiency, PDI, and particle size. The extremities of the response value of each factor correspond to the highest and lowest points on the

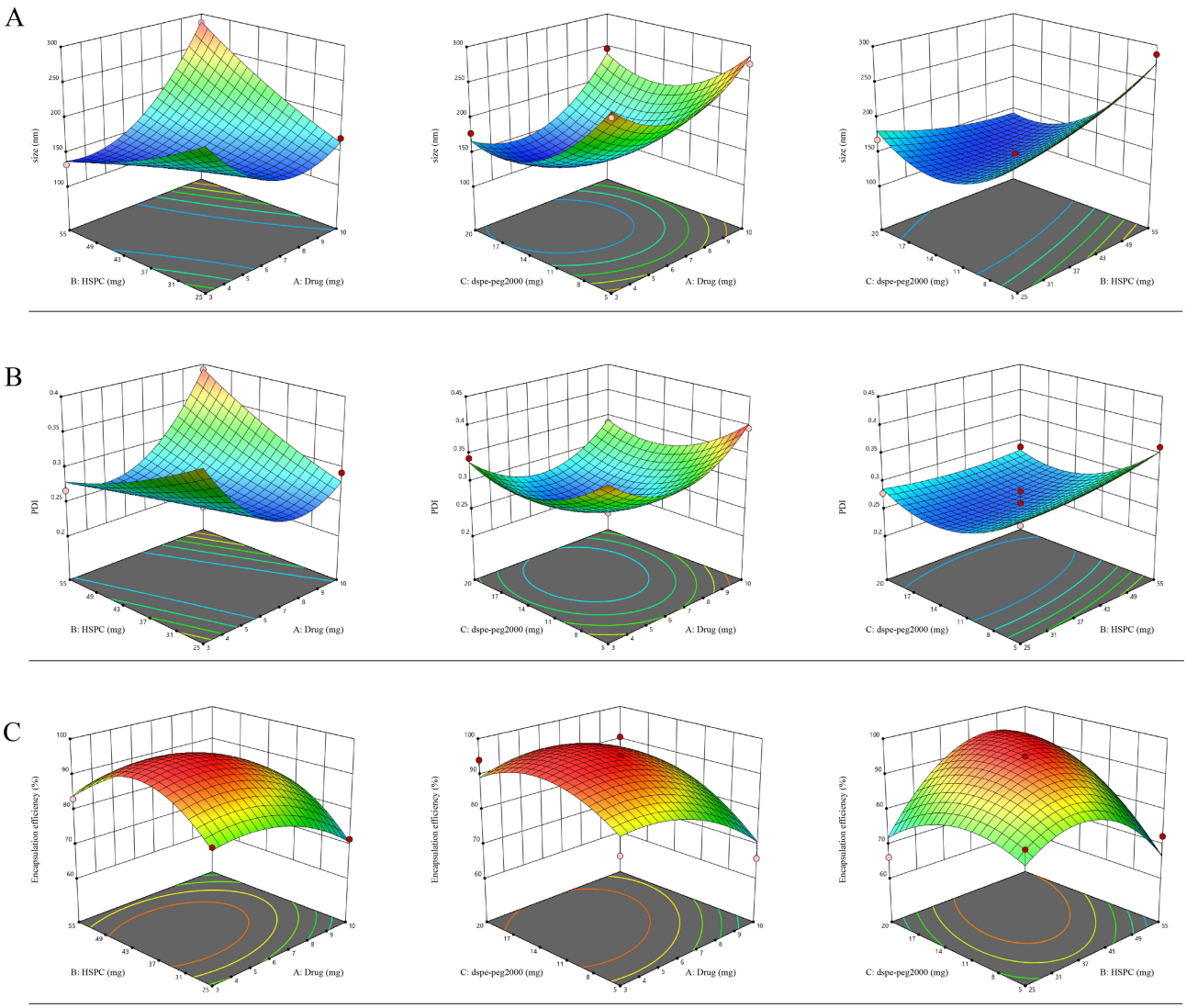

Figure 3 Response surfaces of the effect of three-factor interactions on particle size, PDI, and encapsulation efficiency. Three-dimensional curve map of the effect of three factors on particle size (**A**). Three-dimensional curve map of the effect of three factors on PDI (**B**). Three-dimensional curve map of the effect of three factors on encapsulation efficiency (**C**).

response surface. Based on single-factor analysis, response surface contour maps, and fitted regression equations, the optimal prescription was determined as follows: DSPE-PEG2000 = 13.9 mg; HSPC = 38.5 mg; BAL-PTX = 6.7 mg.

Characterization of BAL-PTX-LN

Using a TEM and particle size analyzer, three batches of BAL-PTX-LN were made in accordance with the final screening prescription. Their morphology, particle size, PDI, and entrapment efficiency were assessed (Figure 4 and Table 5). The data demonstrate that there is little variation between each response value of the anticipated prescription and the actual value, further demonstrating the accuracy of the optimal prescription result produced by the central design-surface optimization model and its optimal prescription quantity.

In vitro Release Behavior of BAL-PTX-LN

The cumulative release of BAL-PTX-LN over 48 h in vitro is depicted in Figure 5A. When BAL and PTX were combined, the cumulative average release rate of PTX in the active pharmaceutical ingredient (API) group was 72.48% at 48 h, lower than that in BAL-PTX-LN (86.62%). Regarding BAL, BAL in the combined API group rapidly released over 40% within 2 h. However, BAL in BAL-PTX-LN exhibited slow and effective drug release compared to the API. The

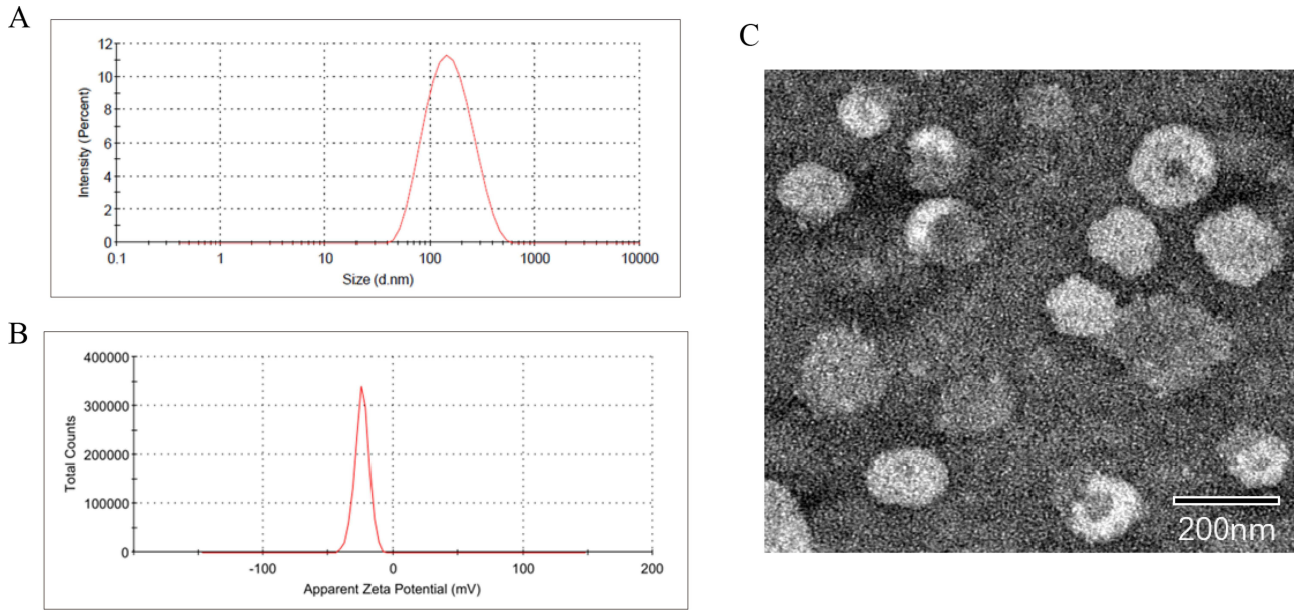

Figure 4 The Characterization of BAL-PTX-LN. The particle size of BAL-PTX-LN (**A**). The Zeta potential of BAL-PTX-LN (**B**). TEM image of BAL-PTX-LN (**C**).

in vitro release behavior of BAL in liposomes aligns more closely with the Higuchi model, whereas its release behavior in APIs resembles the first-order model, indicating diffusion as the primary release mechanism, according to the fitting data of the in vitro release results (Table 6). Overall, liposomes, whether for BAL or PTX, demonstrate a sustained releasing effect.

In vitro Hemolytic Analysis

The results of the hemolysis experiment are presented in Figure 5B and Table 7. The sample in No. 7 (double distilled water, positive control) exhibited full hemolysis, with a hemolysis rate of 9.69 ± 0.44%, whereas the sample in No. 8 (negative control) showed no hemolysis. BAL-PTX-LN at low concentrations (groups 1–3) did not induce changes in appearance or hemolysis rate compared to the negative control group. Similarly, BAL-PTX-LN at middle and high concentrations (groups 4–6) did not demonstrate significant hemolysis, with the maximum hemolysis rate observed at 3.23% ± 0.76% in the high concentration group (group 6), remaining within the safe range of drug-induced hemolysis (below 5%).

Stability Investigation of Preparation

The investigation of solution stability can be seen from Figure 6A. Up to 12 days of cold storage, there was no discernible variation in the BAL-PTX-LN liquid preparation's particle size, PDI, or encapsulation efficiency. Particle size and PDI grew dramatically on the fifteenth day; on the tenth day, they were 125.36 ± 5.35 nm, and on the fifteenth day, they were 149.47 ± 6.03 nm, with a PDI of 0.32 ± 0.02. Simultaneously, the encapsulation efficiency dropped quickly to

Table 5 Comparison Between Design Prescription and Actual Prescription

Response	BAL-PTX-LN	
	Predicted values	Actual values
Y1 (Size nm)	140.03	134.36 ± 3.18
Y2 (PDI)	0.25	0.24 ± 0.02
Y3 (Entrapment efficiency %)	95.12	92.58 ± 2.47

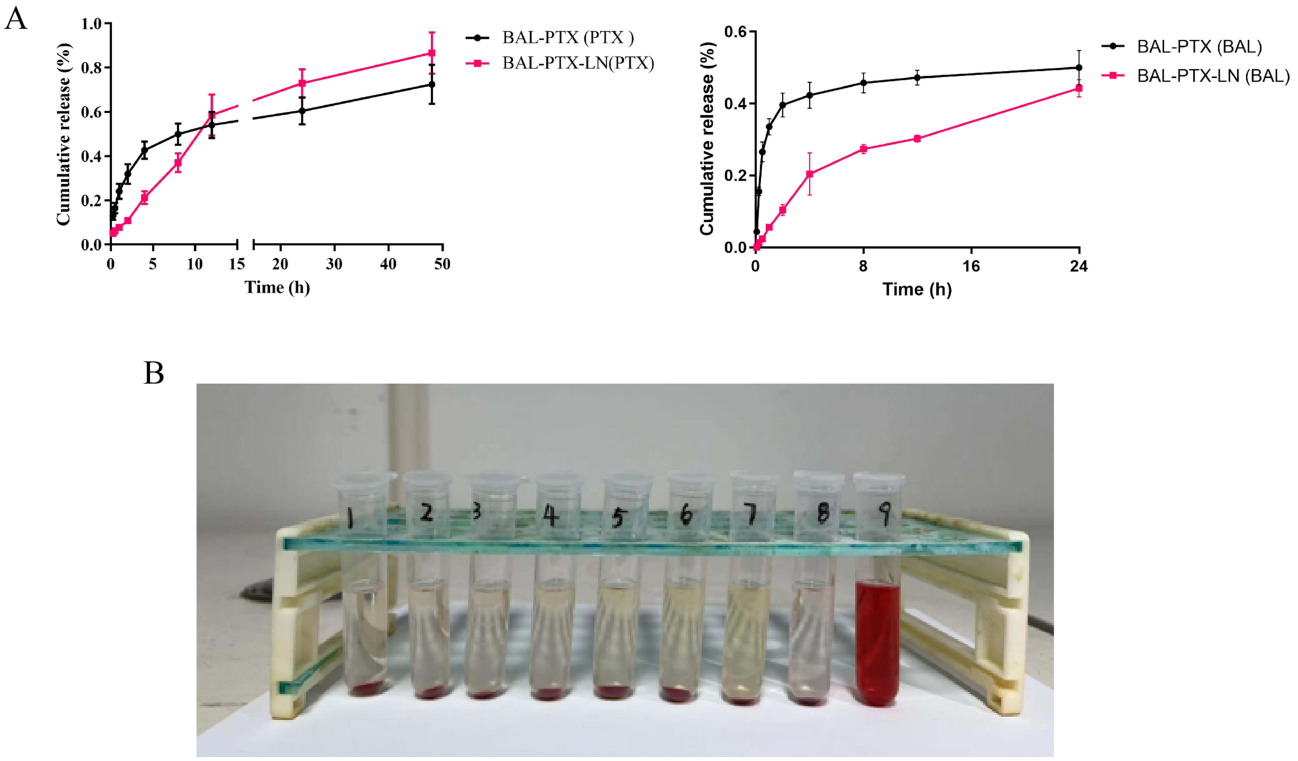

Figure 5 The In vitro release and hemolysis evaluation of BAL-PTX-LN. In vitro release study of BAL-PTX-LN and BAL-PTX (**A**). The hemolysis experiment of BAL-PTX-LN (**B**). ($\bar{x} \pm s$, n = 3).

84.33 ± 5.66% (BAL) and 86.52 ± 5.71% (PTX). Similarly, while the preparation remained stable for 24 h at room temperature, noticeable changes in particle size, PDI, and EE were observed at 48 h (Figure 6B).

Figure 6C shows that, following six months of room temperature storage, the BAL-PTX-LN freeze-dried powder's particle size (143.36 ± 4.66 nm), PDI (0.27 ± 0.03), and encapsulation efficiency (PTX: 92.37 ± 4.75%, BAL: 88.43 ± 3.65%) are essentially the same. However, after nine months, the BAL-PTX-LN freeze-dried powder's encapsulation efficiency dropped to 85.8 ± 6.36% (PTX) and 82.08 ± 5.97% (BAL), despite the fact that its PDI remained consistent at 0.26 ± 0.02. The particle size rose quickly to 189.63 ± 7.37 nm.

In vitro Antitumor Investigation of the Drug Combination

The cytotoxicity of BAL-PTX and BAL-PTX-LN lipid nanoparticles on lung cancer A549 cells, lung cancer H460 cells, and normal human hepatocytes L02 was examined at 24, 48, 72, and 96 h after preparing BAL-PTX (5:1) into lipid nanoparticles BAL-PTX-LN.

Figure 7A illustrates BAL-PTX and BAL-PTX-LN inhibited A549 cell proliferation in concentration- and time-dependent manners. At the same concentration, BAL-PTX-LN exhibited a slightly higher inhibitory rate on A549 cells compared to BAL-PTX. This difference was particularly pronounced at higher concentrations (25 μg/mL and 50 μg/mL)

Table 6 Fit Coefficients of PTX and BAL in Different Release Models

Group	Zero-Order Release Model	First-Order Release Model	Higuchi Model
BAL-PTX (PTX)	0.683	0.792	0.901
BAL-PTX-LN (PTX)	0.931	0.882	0.897
BAL-PTX (BAL)	0.360	0.975	0.621
BAL-PTX-LN (BAL)	0.872	0.881	0.984

Table 7 The Results of the Hemolysis Experiment of BAL-PTX-LN

Number	Volume of BAL-PTX-LN (mL)	2% Saline (mL)	Ultrapure Water (mL)	2% Hematocyte (mL)	Hemolysis
1	0.1	2.4	-	2.5	-
2	0.2	2.3	-	2.5	-
3	0.4	2.1	-	2.5	-
4	0.6	1.9	-	2.5	0.86 ± 0.31
5	0.8	1.7	-	2.5	2.04 ± 0.37
6	1	1.5	-	2.5	3.52 ± 0.83
7	1.2	1.3	-	2.5	9.81 ± 0.48
8	-	2.5	-	2.5	-
9	-	-	2.5	2.5	100

($P < 0.01$). For instance, at 72 h, the inhibition rate of the BAL-PTX-LN group at 25 μg/mL was nearly 40% higher than that of the BAL-PTX group. In general, preparing BAL-PTX as lipid nanoparticles enhanced the sensitivity of drugs to A549 cells and improved its inhibitory effect. As can be seen from Figure 7B, the inhibitory effects of BAL-PTX and BAL-PTX-LN on the proliferation of H460 cells also showed a concentration-dependent and time-dependent manner at

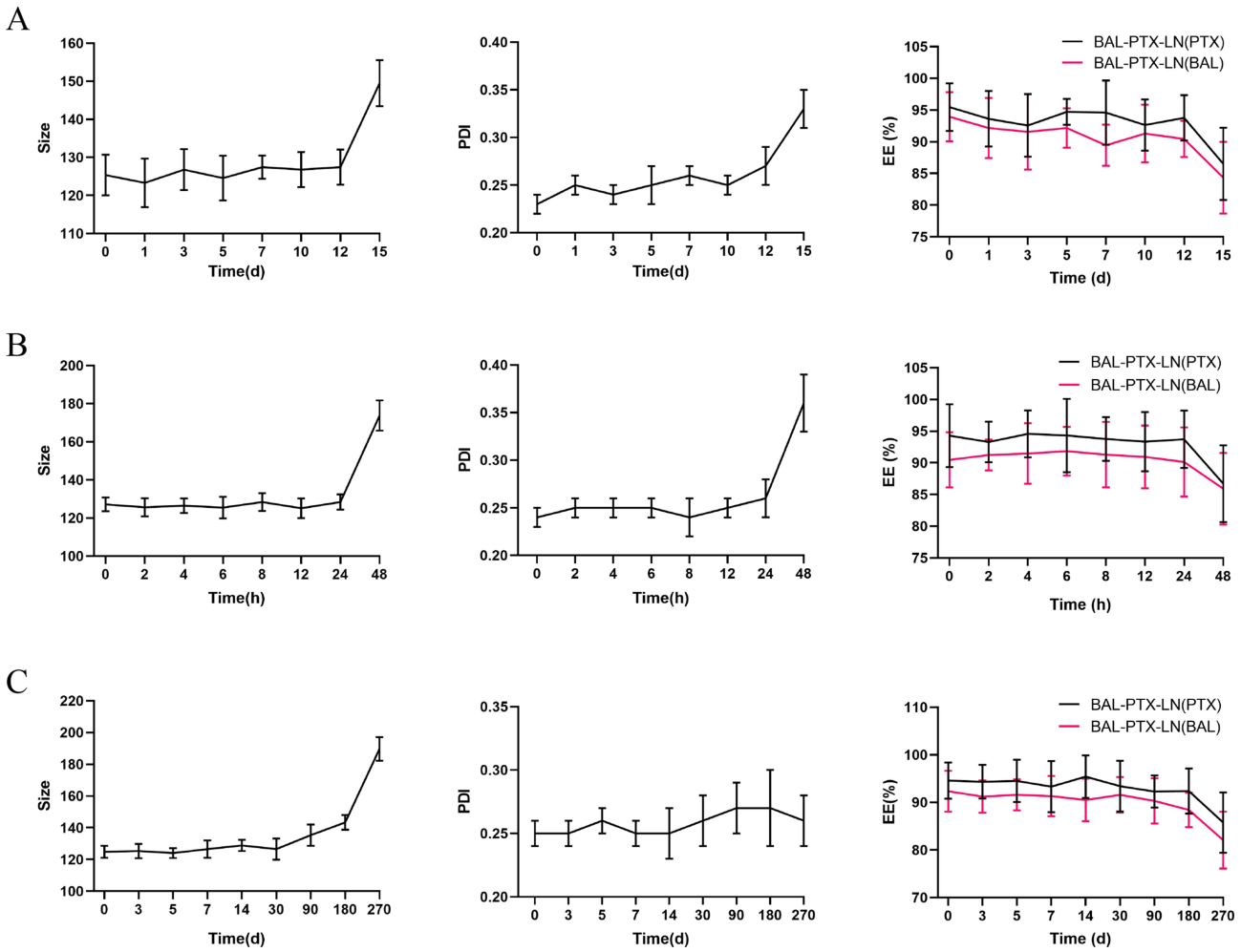

Figure 6 The stability evaluation of BAL-PTX-LN. The stability of BAL-PTX-LN under refrigerated conditions (4°C) (**A**). The stability of BAL-PTX-LN at Room Temperature (25°C) (**B**). Stability of BAL-PTX-LN lyophilized powder at room temperature (25°C) (**C**).($\bar{x} \pm s$ n = 3).

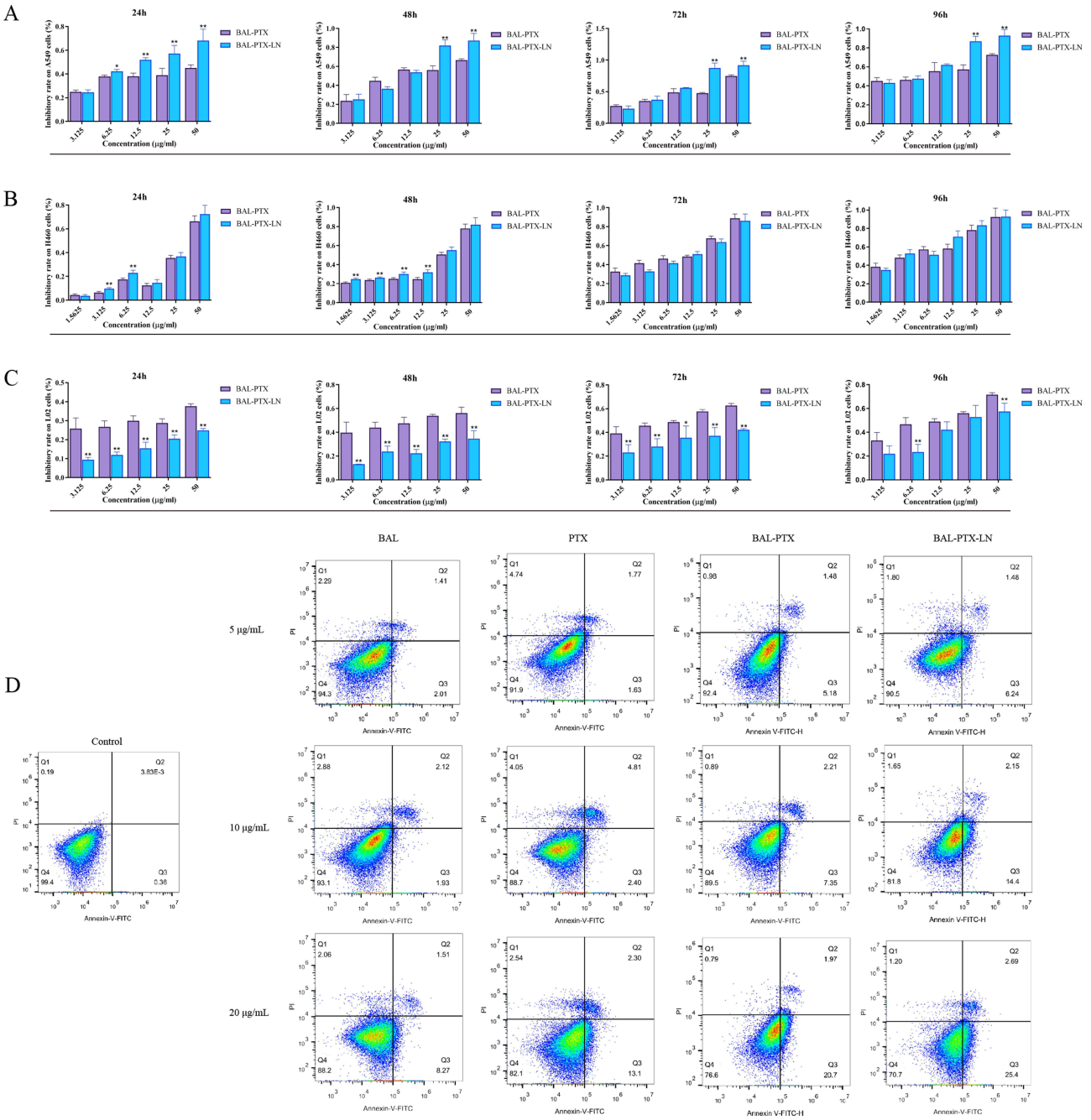

Figure 7 The effect of BAL-PTX-LN lipid nanoparticles on cell viability. The inhibitory rate (%) of A549 cells by BAL-PTX and BAL-PTX-LN at 24 h, 48 h, 72 h and 96 h, respectively (**A**). The inhibitory rate (%) of H460 cells by BAL-PTX and BAL-PTX-LN at 24 h, 48 h, 72 h and 96 h, respectively (**B**). The inhibitory rate (%) of L02 cells by BAL-PTX and BAL-PTX-LN at 24 h, 48 h, 72 h and 96 h, respectively (**C**). Induction of apoptosis of A549 cells by administration groups at different concentrations (**D**). $^{*}P < 0.05 < 0.05$, $^{**}P < 0.05 < 0.01$. ($\bar{x} \pm s$, n = 3).

multiple concentrations. When BAL-PTX-LN was used at lower dosages (1.5625 μg/mL, 3.125 μg/mL, 6.25 μg/mL, and 12.5 μg/mL) in comparison to BAL-PTX, the inhibitory rate on H460 after 24 and 48 hours was considerably higher. However, with the prolongation of administration time, there was no statistical difference between BAL-PTX-LN and BAL-PTX at the same concentration at 72 h and 96 h. As can be seen from Figure 7C, the inhibition rate of BAL-PTX-LN on normal hepatocyte L02 is lower than that of BAL-PTX at almost all concentrations and time points. In summary, A549 cells responded more favorably to the synergistic antitumor action of BAL-PTX. The sensitivity and inhibition rate of BAL-PTX-LN on A549 cells have also been significantly enhanced after being formed into lipid nanoparticles. Thus,

the A549 cell line was chosen for the in vivo construction of a tumor cell model, the detection of tumor cell apoptosis, and the assessment of the effectiveness of anti-lung cancer therapies.

Apoptosis plays a significant role in regulating cell division and proliferation, with inducing apoptosis in cancerous cells being an effective strategy for managing cancer cell growth.[31,32] In the quadrant diagram of apoptosis, Q1 to Q4 represent the necrosis rate, early apoptosis rate, late apoptosis rate, and normal cell survival rate, respectively. As shown in Figure 7D, the apoptosis rates of A549 cells induced by each drug at three concentrations (5 μg/mL, 10 μg/mL, and 20 μg/mL) for 24h were BAL(3.63%, 4.64%, and 10.22%), PTX(3.57%, 7.34%, and 16.6%), and BAL-PTX(7.30%, 9.81%, and 22.51%), respectively. Compared with standalone BAL or PTX, their combination at the same concentration significantly improved the apoptosis of A549 cells ($P < 0.05$). Upon preparation into lipid nanoparticles, BAL-PTX-LN exhibited apoptotic rates of 8.65%, 17.17%, and 29.38% at low, medium, and high concentrations (5 μg/mL, 10 μg/mL, and 20 μg/mL), respectively. While there was no significant difference between the API and preparation groups at low concentrations, the apoptosis effect of the same medium and high-concentration drugs on A549 cells was as follows: BAL-PTX < BAL-PTX-LN ($P < 0.05$).

Pharmacokinetic Studies

All drugs were administered via tail vein injection, and the blood drug concentrations measured at different time points are shown in Table 8. Compared to the BAL-PTX-LN nano-preparation, medications in the bulk drug group metabolized more rapidly in vivo, indicating that the pharmaceuticals in the preparation group exhibit a longer systemic circulation period. By fitting the main pharmacokinetic parameters, it was determined that the pharmacokinetic behavior of PTX in the BAL-PTX raw material group followed a two-compartment model, whereas the behavior of other groups followed a three-compartment model (Table 9). Upon BAL-PTX being formulated into lipid nanoparticles, the bioavailability (area under the curve) of PTX and BAL in rats significantly increased, reaching three times that of the API group. We also noted a significant increase in the retention time (MRT (0-t)). The clearance rate of each drug in the preparation group was 2–3 times lower than that in the API group. In particular, for PTX, the half-life ($t_{1/2z}$) of the BAL-PTX-LN preparation group was 17.124 h, twice as long as that of the BAL-PTX raw material drug group (8.345 h).

In vivo Antitumor Investigation

As shown in the Figure 8D, the body weight of nude mice in all groups—aside from the BAL-PTX-LN preparation group—decreased after 21 days of administration in comparison to the body weight at the start of administration. The control group experienced the greatest decrease among all groups ($P < 0.05$). In contrast, the weight loss of the API groups (PTX, BAL, and BAL-PTX) was gradual. Furthermore, at least one or two nude mice died in the API group and blank

Table 8 Plasma Concentrations of BAL-PTX and BAL-PTX-LN ($\bar{x} \pm s$, n = 5)

Time (min)	BAL-PTX (μg/mL)		BAL-PTX-LN (μg/mL)	
	BAL	PTX	BAL	PTX
5	10.66 ± 2.14	1.79 ± 0.49	19.54 ± 2.64	2.85 ± 0.61
10	5.68 ± 0.69	1.60 ± 0.49	15.72 ± 1.94	2.34 ± 0.37
15	-	1.56 ± 0.29	16.04 ± 1.90	2.08 ± 0.46
30	4.35 ± 0.71	0.89 ± 0.23	8.81 ±1.26	1.63 ± 0.22
60	1.09 ± 0.26	0.36 ± 0.05	7.09 ±1.17	1.01 ± 0.27
120	0.29 ± 0.09	0.36 ± 0.11	1.82 ± 0.27	0.64 ± 0.11
240	0.25 ± 0.04	0.33 ± 0.09	0.93 ± 0.21	0.60 ± 0.07
640	0.26 ± 0.03	0.25 ± 0.05	0.46 ± 0.12	0.54 ± 0.10
720	0.25 ± 0.04	0.13 ± 0.02	0.38 ± 0.07	0.32 ± 0.09
1440	0.14 ± 0.02	0.10 ± 0.01	0.32 ± 0.03	0.23 ± 0.02
2880	-	-	0.14 ± 0.01	0.10 ± 0.01

Table 9 Pharmacokinetic Parameters After Intravenous Injection of BAL-PTX and BAL-PTX-LN in SD Rats

Parameter	Units	BAL-PTX (PTX)	BAL-PTX-LN (PTX)	BAL-PTX (BAL)	BAL-PTX-LN (BAL)
$AUC_{(0-t)}$	mg/L*h	5.425	14.998	10.143	32.991
$MRT_{(0-t)}$	h	7.583	14.301	5.738	8.931
$t_{1/2z}$	h	8.345	17.124	21.946	23.09
T_{max}	h	0.08	0.08	0.08	0.08
C_{max}	mg/L	1.785	2.850	10.660	19.537
CL_z	L/h/kg	1.378	0.57	3.429	1.334
V_z	L/kg	24.543	14.075	108.585	44.442

group. No weight loss or death of nude mice was found in the preparation group after administration. The tumor volume of nude mice in all groups gradually increased to different degrees (Figure 8A–C). The tumor of nude mice in the blank group increased the fastest among them. Compared with the tumor growth trend in the blank group, the drug group exhibited some inhibitory effects on tumor growth. Therefore, the volume and weight of tumors decreased following the combination of BAL and PTX, with corresponding tumor inhibition rates of 29.95%, 45.80%, and 53.24% for PTX, BAL, and BAL-PTX, respectively. Compared with the inhibition rate of BAL-PTX, the inhibition rate of BAL and PTX was statistically significant (BAL-PTX vs BAL $P < 0.05$, BAL-PTX vs PTX $P < 0.0001$). Furthermore, compared with the combined effect of the raw material group, the effect of BAL-PTX-LN was statistically significant, with a tumor inhibition rate of 62.83% (BAL-PTX-LN vs BAL-PTX $P < 0.05$).

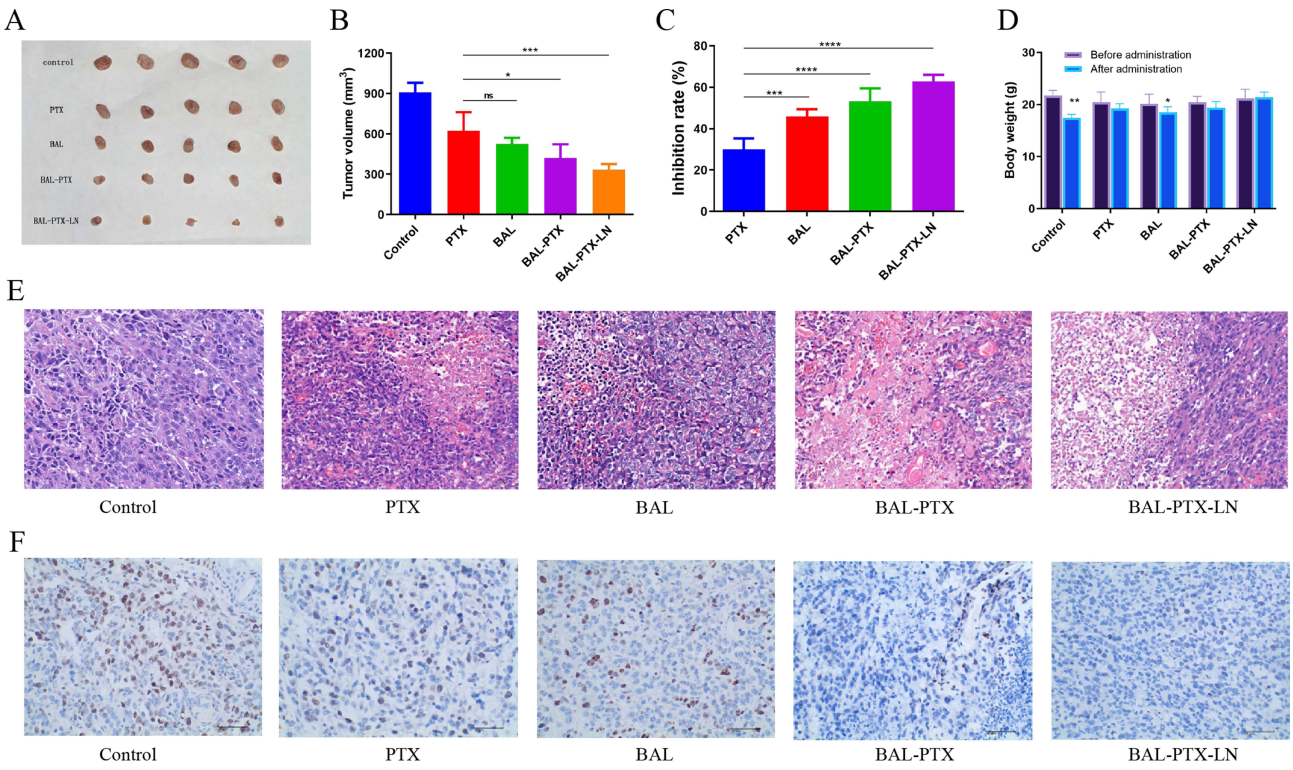

Figure 8 The anti-lung cancer effect of BAL-PTX-LN in vivo. Tumors of nude mice in each group after 21 days of administration (**A**). Tumor volume of nude mice in each administration group after 21 days of administration (**B**). Tumor inhibition rate of each administration group (**C**). Changes in body weight of nude mice (**D**). Pathological HE staining of tumor tissues from mice in each group (**E**). Expression of ki67 in tumor tissues was determined by immunohistochemistry (**F**). *$P < 0.05$, **$P < 0.01$, ***$P < 0.001$, ****$P < 0.0001$. ($\bar{x} \pm s$, n = 5).

HE Staining

After terminating the experiment, the nude mice were killed, and the tumor tissues of each group were analyzed by HE staining and immunohistochemistry. As shown in Figure 8E, the tumor cells in the blank control group exhibited rapidly growing, round, or oval nuclei, and minimal local necrosis was observed between tumor tissues. In the BAL group, sporadic or localized necrosis, accounting for a 15% necrosis rate, was observed between tumor tissues. Apoptotic cells formed a structure resembling a vacuum, and capillary hyperplasia persisted in the intercellular space. In the PTX group, local flaky necrosis was evident in the tumor tissue, with necrosis accounting for approximately 20% of the total area of the tumor tissue. Neutrophils and plasma cells were observed in the necrotic area, along with some cell apoptosis. The BAL-PTX group showed varying degrees of flaky necrosis in tumor tissues, with the necrotic area reaching approximately 50%, accompanied by the presence of numerous tumor cell fragments. Lastly, in the BAL-PTX-LN group, a large area of necrosis was observed in tumor tissues, with more than half of the tumor tissues exhibiting this phenomenon. The necrotic tumor tissue was characterized by the fragmentation of numerous tumor cells, along with the infiltration of neutrophils with rod-shaped or lobulated nuclei and plasma cells with nuclei biased to one side of the cells. Tumor cells in the tumor growth area exhibited irregular arrangement, abundant cytoplasm, atypical nuclei, pathological mitosis, and increased tumor cell apoptosis. Furthermore, immunohistochemistry results indicated that compared with the single drug group, the combination of BAL and PTX significantly downregulated the expression of Ki67 in tumor tissues (< 30%) (Figure 8F). Concurrently, the BAL-PTX-LN group further downregulated the expression of Ki67 in tumor tissue (< 20%), exhibiting a more effective inhibition of tumor proliferation.

The results of the HE staining analysis are shown in Figure 9. Tumor cell infiltration was observed in all organs and the heart, and the mice in the control group and the PTX administration group showed different degrees of pathological changes and necrosis in their hearts and livers. After a prolonged BAL injection, mild inflammation and pathological changes were observed in various organs of the mice. The liver and lung also exhibited different degrees of tumor cell infiltration. After the administration of the drug combination, inflammation, pathological changes, and cell infiltration were not significantly improved in the BAL-PTX administration group. Nevertheless, after the administration of the prepared lipid nano-drug delivery system, BAL-PTX-LN mice showed almost no distinct pathological changes, and only a few neutrophils were found in the lungs.

Discussion

PTX is known to exert its anticancer effects by promoting the polymerization and stability of microtubules, thereby blocking cells in the metaphase of bipolar spindles.[33] Additionally, PTX can cause DNA damage, induce oxidative stress, and trigger apoptosis, indicating that it may use other cytotoxic mechanisms.[34] PTX functions through the PI3K/Akt intracellular signal transduction pathway, which plays a crucial role in PTX-induced drug resistance.[17] Aberrant activity in the AKT/mTOR pathway and its downstream signaling cascade is associated with migration, adhesion, angiogenesis, extracellular matrix degradation, malignant transformation of cancer cells, angiogenesis, cell cycle progression, and apoptosis.[35,36] Akt, at the center of this pathway, phosphorylates downstream substrates to regulate the expression of target genes.[37,38] Chiral compounds with a lactam structure can promote the apoptosis of cancer cells by inhibiting Akt phosphorylation. This upregulates the expression of caspase-3 and caspase-9 while downregulating the expression of Bcl-2.[39]

BAL, created through the establishment of an amide bond between BA and PMEs, can block the PI3K/AKT pathway.[15] In a xenograft tumor model with an overactivated PI3K/AKT signaling pathway, our previous findings have shown that BAL significantly inhibits the AKT/mTOR signaling pathway, leading to significant suppression of cell proliferation, induction of cell stress, G1 phase arrest, apoptosis, and ultimately manifesting a potent anti-tumor effect. In the present study, we investigated the potential synergy between BAL and PTX. In the calculation and analysis of the CI value, which serves as the combination index, a CI value greater than 1 indicates antagonistic effects between the two drugs, a CI value equal to 1 suggests additive drug effects, and a CI value less than 1 indicates synergistic effects from the combination of the two drugs. Through comparative analysis, we confirmed that the combination of BAL and PTX

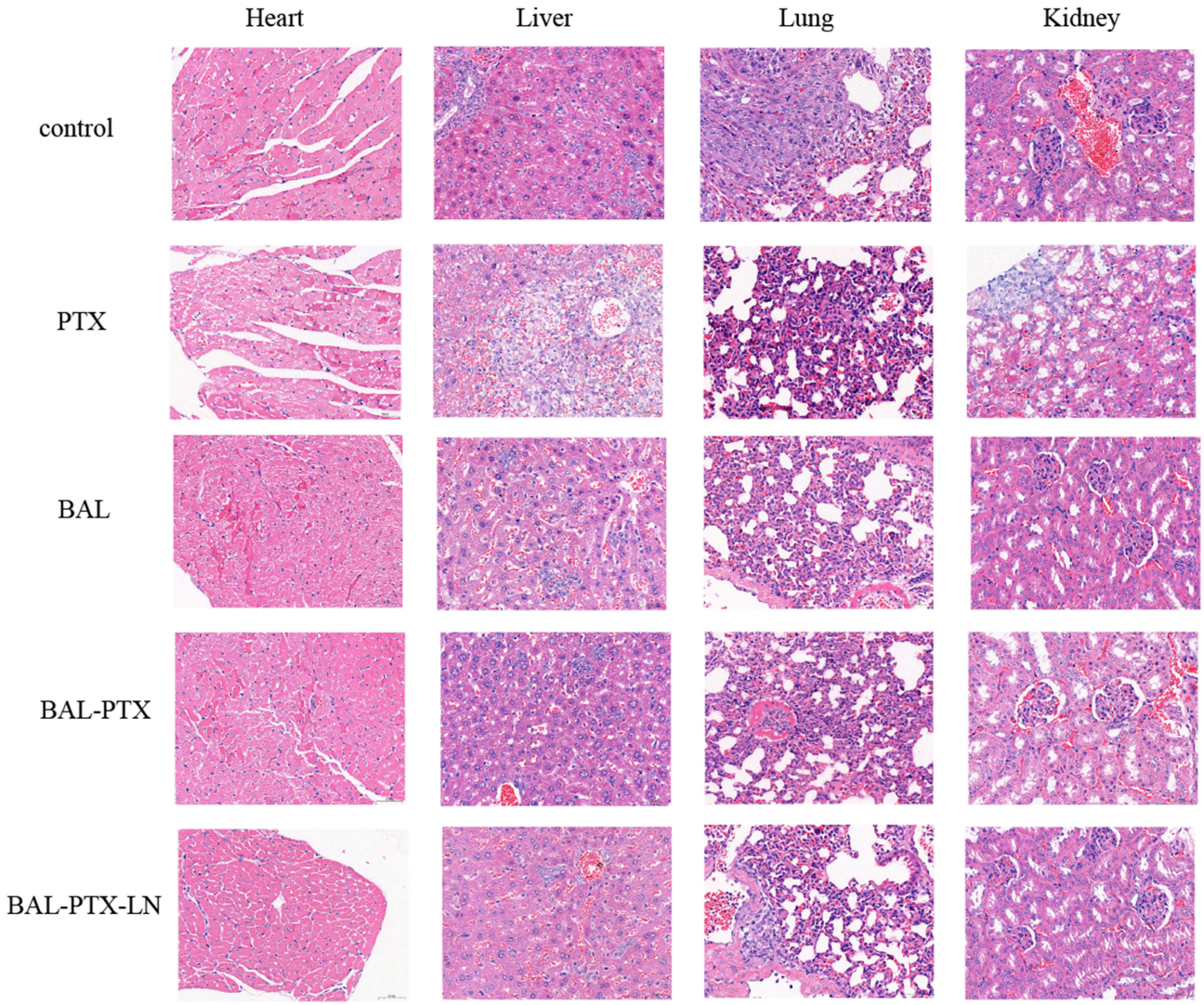

Figure 9 Pathological HE staining of heart, liver, kidney and lung tissues from mice in each group.

synergistically inhibits the growth of lung cancer A549 cells and H460 cells, inducing their apoptosis. Importantly, we found that the combination with a mass ratio of 5:1 exhibits the strongest synergistic effect.

BAL-PTX has some limitations, such as low bioavailability and poor solubility.[22,23] Following the screening of synergistic ratios, we developed lipid nanoparticles and performed subsequent experiments. The particle size of the BAL-PTX-LN sample was found to be 134.36 ± 3.18 nm through a single-factor experiment and CCD central combination optimization. The nanoparticles exhibited a homogeneous and spherical particle size distribution, without apparent signs of aggregation. Nanoparticles of the appropriate size exhibit passive targeting capabilities. Due to the EPR effect, cancer blood vessels can spread more widely within tumor tissues because their capillary gap is larger than 400 nm.[40] The surface of BAL-PTX-LN is negatively charged, with a zeta potential of 23.9 ± 1.67 mV. This electrostatic repulsion increases the distance between particles, decreasing nanoparticle aggregation.[41–43] Additionally, during the initial 12 days, the particle size, PDI, and encapsulation efficiency of the BAL-PTX-LN liquid preparation showed no significant differences under cold storage conditions. However, on day 15, the particle size and PDI of the preparation significantly increased, and its encapsulation efficiency decreased from 90% to approximately 80%. This indicates a certain level of stability in the liquid preparation but highlights the need for improvement. Freeze-drying technology can address this limitation and improve the stability of lipid nanoparticles.[44,45] After six months of room temperature storage, the freeze-dried powder exhibited no significant changes in particle size, PDI, or entrapment efficiency. It is unclear whether the

freeze-dried sample can be kept at room temperature for an extended period of time, even though the entrapment efficiency of the BAL-PTX-LN freeze-dried powder showed a decreasing trend after nine months. Nevertheless, no significant difference was found ($P > 0.05$), suggesting good stability of the freeze-dried powder system.

BAL-PTX-LN, a lipid nano-delivery system, has a strong inhibitory effect on lung cancer cells A549 and H460 at the cellular level. Comparatively, the combination of BAL-PTX shows an increased capacity to induce apoptosis in A549 cells compared with individual effects of BAL or PTX alone. This improved effect is achieved more with the use of lipid nanoparticles in BAL-PTX-LN, further demonstrating that the preparation group's impact outweighed the direct mixing of raw ingredients. Notably, in contrast to the effect on lung cancer cells A549 and H460, the API group showed a stronger inhibitory effect on normal liver cells L02 compared with the preparation group. This suggests that BAL-PTX-LN improves the selective ability of the drug to target and kill lung cancer cells while decreasing their effect on normal cells. Furthermore, it suggests that BAL-PTX-LN exhibits a certain degree of safety compared with BAL-PTX.

Red blood cell injections are typically tested for biocompatibility before usage. The findings from our study indicate that BAL-PTX-LN with a concentration less than 200 μg/mL hardly causes hemolysis. In clinical practice, free PTX is dissolved using ethanol and hydrogenated castor oil for simple administration.[46] However, this solvent can lead to significant hemolysis, which can be effectively avoided with the lipid nanoparticles developed in our work. Lipid nanoparticles extend the half-lives of PTX and BAL, raise the area under the drug-time curve, enhance the relative bioavailability of medications, and lower the in vivo clearance rate, according to the results of pharmacokinetic studies. This indicates that compared to BAL-PTX-LN nano-preparation, the medication in the BAL-PTX bulk drug group requires less time to metabolize in vivo. While its hydrophilic portion protects space and increases the water solubility of insoluble pharmaceuticals, HSPC's hydrophobic core functions as an amphoteric surfactant, capable of carrying highly insoluble medications with high loading.[47] An auxiliary substance with benefits for long-term circulation is DSPE-PEG2000. The extended residence duration in vivo and improved relative bioavailability of the aforementioned medications may be attributed to the excipients' characteristics, as DSPE-PEG2000 is included in the prescription of lipid nanoparticles.[48–50] In general, the preparation's enhancement of pharmacokinetic behavior serves as a foundation for the improvement of in vivo efficacy that follows.

A subcutaneously implanted tumor model was constructed to further study the pharmacodynamics of combination treatment.[51,52] The body weight of nude mice from all groups (except those in the BAL-PTX-LN preparation group) decreased in in vivo pharmacodynamic trials compared with their body weight at the start of treatment. Furthermore, the control group exhibited the largest decrease ($P < 0.05$). This indicates that the survival status of mice in the later stages of treatment was affected by the large subcutaneous tumor volume. The expression of Ki67 was significantly downregulated in tissues and the growth of tumor volume and weight was suppressed in all dosing groups compared with those in the blank group.[53–55] When BAL and PTX are combined, the anti-lung cancer effect in vivo is significantly improved compared with single-drug delivery. Additionally, when BAL and PTX are combined, the anti-lung cancer effect of the BAL-PTX co-loaded lipid nano-drug delivery system is further enhanced. This indicates that the combination of BAL and PTX does have a significant synergistic anti-tumor effect, and that effect is also more strongly reflected in its liposomes. Notably, one or two naked mice died in each API group but not in the pretreatment group. Given that the API group is quite hazardous, we believe that anhydrous ethanol and castor oil may be employed as mixed solvents for injection. Because of its increased solubility, our preparation group uses the water-soluble version, avoiding this harmful effect. Simultaneously, the preparation group exhibits higher safety than the API group at the cellular level; therefore, it is not surprising that there is not a single nude mouse death in the preparation group, but rather in the API group, which is another crucial example of how safety has greatly increased following our preparation optimization. In summary, pharmacodynamic studies conducted in vivo provided additional evidence that BAL and PTX collaborated to prevent tumor growth and promote anti-tumor proliferation. Meanwhile, advancements in pharmaceutics improved the way these drugs performed.

While the in vivo efficacy was confirmed, we further investigated the safety of the preparation. Pathological analysis after HE staining indicated that the toxicity of co-loaded lipid nanoparticles to different organs was very slight compared with that of single drug and free drug. Furthermore, inflammation and tumor cell infiltration were not found in the organs

of the single drug group and combined drug group.[56,57] It can be inferred that the lipid nanoparticle delivery system containing BAL and PTX exhibits good safety and can effectively alleviate the invasion of tumor cells.

Conclusion

The findings of the present study show that the combination of the novel chiral baicalin derivative BAL and PTX has a significant synergistic antitumor effect in vitro and in vivo. The pharmacokinetics and drug release profile of BAL-PTX -LN are favorable. Spherical co-loaded lipid nanoparticles BAL-PTX-LN were successfully prepared, with high EE, optimal particle size and PDI. BAL-PTX-LN could effectively suppress lung cancer cell proliferation while also inducing apoptosis, significantly improving anti-tumor activity in vivo and in vitro. Simultaneously, BAL-PTX-LN exhibits good biocompatibility and is not harmful to normal tissues. Altogether, the development of the BAL-PTX-LNP lipid nano-co-delivery system provides a novel direction for safer and more effective treatment of lung cancer.

Abbreviations

API, Active pharmaceutical ingredients; BA, Baicalin; CCD, Central Composite Design; CI, Combination index; DSPE-PEG2000, 1.2-dis-tearoyl-sn-glycero-3-phosphoethanolamine-N-[methoxy (poly-ethylene glycol)-2000]; OD, Optical density; EE, Entrapment efficiency; HE, Hematoxylin and eosin; HSPC, Hydrogenated soybean phospholipids; LE, Loading efficiency; PTX, Paclitaxel; TEM, Transmission electron microscopy.

Data Sharing Statement

We will support data and materials on request.

Ethics Approval and Consent to Participate

The animal studies were done in compliance with the regulations and guidelines of Southwest Medical University institutional animal care and adhered to the ARRIVE guidelines. All animal experiments were approved (No. 2020335) by the Ethics Committee of Southwest Medical University.

Author Contributions

All authors made a significant contribution to the work reported, whether that is in the conception, study design, execution, acquisition of data, analysis and interpretation, or in all these areas; took part in drafting, revising or critically reviewing the article; gave final approval of the version to be published; have agreed on the journal to which the article has been submitted; and agree to be accountable for all aspects of the work.

Funding

This study was supported by the Cooperation Project of Chunhui Plan of the Ministry of Education of China (No. HZKY20220563), Sichuan Science and Technology Program (No. 2022YFS0619, 2022YFS0630, 2022YFS0635), the Key R&D Project of Luzhou-Southwest Medical University (No. 2023LZXNYDHZ002), the Cooperation Projects of Sichuan Credit Pharmaceutical CO., Ltd., Central Nervous System Drug Key Laboratory of Sichuan Province (No.210027-01SZ, 200017-01SZ, 230007-01SZ), the Chongqing Traditional Chinese Medicine Inheritance and Innovation Team Construction Project "Traditional Chinese Medicine New Drug and Safety Research Inheritance and Innovation Team" (No.2022-8), the Key R&D Project of Sichuan University-Luzhou (No.2022CDLZ-10), Luzhou Science and Technology Plan Project (No. 2023JYJ034, 2023JYJ022), the Student Innovation and Entrepreneurship Program of Southwest Medical University (No.2023495, 2023497).

Disclosure

The authors declare no conflicts of interest in this work.

References

1. Sung H, Ferlay J, Siegel R, et al. Global cancer statistics 2020: GLOBOCAN estimates of incidence and mortality worldwide for 36 cancers in 185 countries. *Ca a Cancer J Clinicians*. 2021;71(3):209–249. doi:10.3322/caac.21660
2. Siegel R, Miller K, Wagle N, Jemal A. Cancer statistics, 2023. *Ca a Cancer J Clinicians*. 2023;73(1):17–48. doi:10.3322/caac.21763
3. Leiter A, Veluswamy R, Wisnivesky J. The global burden of lung cancer: current status and future trends. *Nat Rev Clin Oncol*. 2023;20(9):624–639. doi:10.1038/s41571-023-00798-3
4. Megyesfalvi Z, Gay C, Popper H, et al. Clinical insights into small cell lung cancer: tumor heterogeneity, diagnosis, therapy, and future directions. *Ca a Cancer J Clinicians*. 2023;73(6):620–652. doi:10.3322/caac.21785
5. Altorki N, Wang X, Kozono D, et al. Lobar or sublobar resection for peripheral stage ia non-small-cell lung cancer. *New Engl J Med*. 2023;388 (6):489–498. doi:10.1056/NEJMoa2212083
6. Wang W, Wang J, Liu S, et al. An EHMT2/NFYA-ALDH2 signaling axis modulates the RAF pathway to regulate paclitaxel resistance in lung cancer. *Mol Cancer*. 2022;21(1):106. doi:10.1186/s12943-022-01579-9
7. Li J, Zhu L, Kwok H. Nanotechnology-based approaches overcome lung cancer drug resistance through diagnosis and treatment. *Drug Resist Updates*. 2023;66:100904. doi:10.1016/j.drup.2022.100904
8. Rugo H, Barry W, Moreno-Aspitia A, et al. Randomized phase III trial of paclitaxel once per week compared with nanoparticle albumin-bound nab-paclitaxel once per week or ixabepilone with bevacizumab as first-line chemotherapy for locally recurrent or metastatic breast cancer: CALGB 40502/NCCTG N063H (alliance). *J Clin Oncol off J Am Soc Clin Oncol*. 2015;33(21):2361–2369. doi:10.1200/JCO.2014.59.5298
9. Chihara Y, Yoshimura A, Date K, et al. Phase II study of S-1 and paclitaxel combination therapy in patients with previously treated non-small cell lung cancer. *Oncologist*. 2019;24(8):1033–e1617. doi:10.1634/theoncologist.2019-0290
10. Zhang L, Zhu L, Yao X, et al. Paclitaxel treatment enhances lymphatic metastasis of B16F10 melanoma cells via CCL21/CCR7 axis. *Int J Bio Sci*. 2022;18(4):1476–1490. doi:10.7150/ijbs.67138
11. Reguera-Nuñez E, Xu P, Chow A, Man S, Hilberg F, Kerbel R. Therapeutic impact of nintedanib with paclitaxel and/or a PD-L1 antibody in preclinical models of orthotopic primary or metastatic triple negative breast cancer. *J Exp Clin Cancer Res*. 2019;38(1):16. doi:10.1186/s13046-018-0999-5
12. Wei Y, Wei Y, Sheng L, et al. Construction of curcumin and paclitaxel co-loaded lipid nano platform and evaluation of its anti-hepatoma activity in vitro and pharmacokinetics in vivo. *Int J Nanomed*. 2023;18:2087–2107. doi:10.2147/IJN.S399289
13. Yadav P, Saklani R, Tiwari A, et al. Ratiometric codelivery of paclitaxel and baicalein loaded nanoemulsion for enhancement of breast cancer treatment. *Int J Pharm*. 2023;643:123209. doi:10.1016/j.ijpharm.2023.123209
14. Nguyen D, Nguyen T, Dinh V, et al. Potential from synergistic effect of quercetin and paclitaxel co-encapsulated in the targeted folic-gelatin-pluronic P123 nanogels for chemotherapy. *Int J Biol Macromol*. 2023;243:125248. doi:10.1016/j.ijbiomac.2023.125248
15. Hou Y, Pi C, Feng X, et al. In vivo antitumor activity and of new chiral derivatives of baicalin and induced apoptosis via the PI3K/Akt signaling pathway. *Mol Ther Oncolytics*. 2020;19:67–78. doi:10.1016/j.omto.2020.08.018
16. Jiménez-López J, El-Hammadi M, Ortiz R, et al. A novel nanoformulation of PLGA with high non-ionic surfactant content improves in vitro and in vivo PTX activity against lung cancer. *Pharmacol Res*. 2019;141:451–465. doi:10.1016/j.phrs.2019.01.013
17. Smith E, Wang J, Yang D, Xu X. Paclitaxel resistance related to nuclear envelope structural sturdiness. *Drug Resist Updates*. 2022;65:100881. doi:10.1016/j.drup.2022.100881
18. Abu-Izneid T, Rauf A, Shariati M, et al. Sesquiterpenes and their derivatives-natural anticancer compounds: an update. *Pharmacol Res*. 2020;161:105165. doi:10.1016/j.phrs.2020.105165
19. Keith C, Borisy A, Stockwell B. Multicomponent therapeutics for networked systems. *Nat Rev Drug Discov*. 2005;4(1):71–78. doi:10.1038/nrd1609
20. Bariwal J, Ma H, Altenberg G, Liang H. Nanodiscs: a versatile nanocarrier platform for cancer diagnosis and treatment. *Chem Soc Rev*. 2022;51 (5):1702–1728. doi:10.1039/D1CS01074C
21. Palmer A, Chidley C, Sorger P. A curative combination cancer therapy achieves high fractional cell killing through low cross-resistance and drug additivity. *eLife*. 2019;8: e50036.
22. Liu C, Liu W, Liu Y, et al. Versatile flexible micelles integrating mucosal penetration and intestinal targeting for effectively oral delivery of paclitaxel. *Acta pharmaceutica Sinica B*. 2023;13(8):3425–3443. doi:10.1016/j.apsb.2023.05.029
23. Stage T, Bergmann T, Kroetz D. Clinical pharmacokinetics of paclitaxel monotherapy: an updated literature review. *Clin Pharmacokinet*. 2018;57 (1):7–19. doi:10.1007/s40262-017-0563-z
24. Kim S, Puranik N, Yadav D, Jin J, Lee P. Lipid nanocarrier-based drug delivery systems: therapeutic advances in the treatment of lung cancer. *Int J Nanomed*. 2023;18:2659–2676. doi:10.2147/IJN.S406415
25. Abousalman-Rezvani Z, Refaat A, Dehghankelishadi P, Roghani-Mamaqani H, Esser L, Voelcker N. Insights into targeted and stimulus-responsive nanocarriers for brain cancer treatment. *Adv Healthcare Mater.* 2024;13(12):e2302902. doi:10.1002/adhm.202302902
26. Graván P, Aguilera-Garrido A, Marchal J, Navarro-Marchal S, Galisteo-González F. Lipid-core nanoparticles: classification, preparation methods, routes of administration and recent advances in cancer treatment. *Adv Colloid Interface Sci*. 2023;314:102871. doi:10.1016/j.cis.2023.102871
27. Ali E, Sharker S, Islam M, et al. Targeting cancer cells with nanotherapeutics and nanodiagnostics: current status and future perspectives. *Semi Cancer Biol*. 2021;69:52–68. doi:10.1016/j.semcancer.2020.01.011
28. Lim S, Sa J, Lee D, et al. Systematic evaluation of gastric tumor cell index and two-drug combination therapy via 3-dimensional high-throughput drug screening. *Front Oncol*. 2019;9:1327. doi:10.3389/fonc.2019.01327
29. Zhang N, Fu J, Chou T. Synergistic combination of microtubule targeting anticancer fludelone with cytoprotective panaxytriol derived from panax ginseng against MX-1 cells in vitro: experimental design and data analysis using the combination index method. *Am J Cancer Res*. 2016;6(1):97–104.
30. Chou T. Drug combination studies and their synergy quantification using the Chou-Talalay method. *Cancer Res*. 2010;70(2):440–446. doi:10.1158/0008-5472.CAN-09-1947
31. Xu X, Lai Y, Hua Z. Apoptosis and apoptotic body: disease message and therapeutic target potentials. *Biosci Rep*. 2019;39: BSR20180992.
32. Hadian K, Stockwell B. The therapeutic potential of targeting regulated non-apoptotic cell death. *Nat Rev Drug Discov*. 2023;22(9):723–742. doi:10.1038/s41573-023-00749-8

33. Zhao S, Tang Y, Wang R, Najafi M. Mechanisms of cancer cell death induction by paclitaxel: an updated review. *Apoptosis*. 2022;27(9–10):647–667. doi:10.1007/s10495-022-01750-z
34. Lin Y, Lin T, Chen C, et al. Enhancing efficacy of albumin-bound paclitaxel for human lung and colorectal cancers through autophagy receptor sequestosome 1 (SQSTM1)/p62-mediated nanodrug delivery and cancer therapy. *ACS nano*. 2023;17(19):19033–19051. doi:10.1021/acsnano.3c04739
35. Glaviano A, Foo A, Lam H, et al. PI3K/AKT/mTOR signaling transduction pathway and targeted therapies in cancer. *Mol Cancer*. 2023;22(1):138. doi:10.1186/s12943-023-01827-6
36. Su W, Tian L, Guo L, Huang L, Gao W. PI3K signaling-regulated metabolic reprogramming: from mechanism to application. *Biochim Biophys Acta Rev Cancer*. 2023;1878(5):188952. doi:10.1016/j.bbcan.2023.188952
37. Tsai P, Lai Y, Manne R, Tsai Y, Sarbassov D, Lin H. Akt: a key transducer in cancer. *J Biomed Sci*. 2022;29(1):76. doi:10.1186/s12929-022-00860-9
38. Vasan N, Cantley L. At a crossroads: how to translate the roles of PI3K in oncogenic and metabolic signalling into improvements in cancer therapy. *Nat Rev Clin Oncol*. 2022;19(7):471–485. doi:10.1038/s41571-022-00633-1
39. Hwang S, Park H, Park Y, Lee H. An α-quaternary chiral latam derivative, YH-304 as a novel broad-spectrum anticancer agent. *Int J Oncol*. 2016;49(6):2480–2486. doi:10.3892/ijo.2016.3726
40. Padhi S, Kapoor R, Verma D, Panda A, Iqbal Z. Formulation and optimization of topotecan nanoparticles: in vitro characterization, cytotoxicity, cellular uptake and pharmacokinetic outcomes. *J Photochem Photobiol B Biol*. 2018;183:222–232. doi:10.1016/j.jphotobiol.2018.04.022
41. Win K, Feng S. Effects of particle size and surface coating on cellular uptake of polymeric nanoparticles for oral delivery of anticancer drugs. *Biomaterials*. 2005;26(15):2713–2722. doi:10.1016/j.biomaterials.2004.07.050
42. Gong X, Zheng Y, He G, Chen K, Zeng X, Chen Z. Multifunctional nanoplatform based on star-shaped copolymer for liver cancer targeting therapy. *Drug Delivery*. 2019;26(1):595–603. doi:10.1080/10717544.2019.1625467
43. Banerjee A, Qi J, Gogoi R, Wong J, Mitragotri S. Role of nanoparticle size, shape and surface chemistry in oral drug delivery. *J Control Release*. 2016;238:176–185. doi:10.1016/j.jconrel.2016.07.051
44. Niu L, Panyam J. Freeze concentration-induced PLGA and polystyrene nanoparticle aggregation: imaging and rational design of lyoprotection. *J Control Release*. 2017;248:125–132. doi:10.1016/j.jconrel.2017.01.019
45. Abdelwahed W, Degobert G, Stainmesse S, Fessi H. Freeze-drying of nanoparticles: formulation, process and storage considerations. *Adv Drug Delivery Rev*. 2006;58(15):1688–1713. doi:10.1016/j.addr.2006.09.017
46. Gradishar W, Tjulandin S, Davidson N, et al. Phase III trial of nanoparticle albumin-bound paclitaxel compared with polyethylated castor oil-based paclitaxel in women with breast cancer. *J Clin Oncol off J Am Soc Clin Oncol*. 2005;23(31):7794–7803. doi:10.1200/JCO.2005.04.937
47. Bhatt R, Singh D, Prakash A, Mishra N. Development, characterization and nasal delivery of rosmarinic acid-loaded solid lipid nanoparticles for the effective management of Huntington's disease. *Drug Delivery*. 2015;22(7):931–939. doi:10.3109/10717544.2014.880860
48. Yoshizawa Y, Kono Y, Ogawara K, Kimura T, Higaki K. PEG liposomalization of paclitaxel improved its in vivo disposition and anti-tumor efficacy. *Int J Pharm*. 2011;412(1–2):132–141. doi:10.1016/j.ijpharm.2011.04.008
49. Che J, Okeke C, Hu Z, Xu J. DSPE-PEG: a distinctive component in drug delivery system. *Curr Pharm Des*. 2015;21(12):1598–1605. doi:10.2174/1381612821666150115144003
50. Cheng Y, Liu M, Hu H, Liu D, Zhou S. Development, optimization, and characterization of pegylated nanoemulsion of prostaglandin E1 for long circulation. *AAPS Pharm Sci Tech*. 2016;17(2):409–417. doi:10.1208/s12249-015-0366-1
51. Navaridas R, Vidal-Sabanés M, Ruiz-Mitjana A, et al. In vivo intra-uterine delivery of tat-fused cre recombinase and CRISPR/Cas9 editing system in mice unveil histopathology of Pten/p53-deficient endometrial cancers. *Adv Sci*. 2023;10(32):e2303134. doi:10.1002/advs.202303134
52. Martinez-Ruiz L, Florido J, Rodriguez-Santana C, et al. Intratumoral injection of melatonin enhances tumor regression in cell line-derived and patient-derived xenografts of head and neck cancer by increasing mitochondrial oxidative stress. *Biomed Pharmacother*. 2023;167:115518. doi:10.1016/j.biopha.2023.115518
53. Li L, Jiang G, Chen Q, Zheng J. Ki67 is a promising molecular target in the diagnosis of cancer (review). *Mol Med Rep*. 2015;11(3):1566–1572. doi:10.3892/mmr.2014.2914
54. Reid M, Bagci P, Ohike N, et al. Calculation of the Ki67 index in pancreatic neuroendocrine tumors: a comparative analysis of four counting methodologies. *Mod Pathol*. 2015;28(5):686–694. doi:10.1038/modpathol.2014.156
55. Bologna-Molina R, Mosqueda-Taylor A, Molina-Frechero N, Mori-Estevez A, Sánchez-Acuña G. Comparison of the value of PCNA and Ki-67 as markers of cell proliferation in ameloblastic tumors. *Med Oral Patologia Oral y Cirugia Bucal*. 2013;18:e174–179. doi:10.4317/medoral.18573
56. Pang Z, Chen X, Wang Y, et al. Comprehensive analyses of the heterogeneity and prognostic significance of tumor-infiltrating immune cells in non-small-cell lung cancer: development and validation of an individualized prognostic model. *Int Immunopharmacol*. 2020;86:106744. doi:10.1016/j.intimp.2020.106744
57. Li H, Wang S, Lian Z, Deng S, Yu K. Relationship between tumor infiltrating immune cells and tumor metastasis and its prognostic value in cancer. *Cells*. 2022;12(1):12. doi:10.3390/cells12010012